Atmos. Chem. Phys. Discuss., https://doi.org/10.5194/acp-2018-1193
Manuscript under review for journal Atmos. Chem. Phys.
Discussion started: 12 December 2018

Atmospheric Chemistry and Physics Discussions

Mechanism of ozone loss under enhanced water vapour conditions in the mid-latitude lower stratosphere in summer

Sabine Robrecht[1], Bärbel Vogel[1], Jens-Uwe Grooß[1], Karen Rosenlof[2], Troy Thornberry[2,3], Andrew Rollins[2], Martina Krämer[1], Lance Christensen[4], and Rolf Müller[1]

[1]Forschungszentrum Jülich, Institute of Energy and Climate Research (IEK-7), Jülich, Germany
[2]NOAA Earth System Research Laboratory (ESRL) Chemical Sciences Division, Boulder, CO 80305 USA
[3]University of Colorado, Cooperative Institute for Research in Environmental Sciences, Boulder, CO 80309 USA
[4]California Institute of Technology, Jet Propulsion Laboratory, Pasadena, CA 91125 USA

Correspondence to: Sabine Robrecht (sa.robrecht@fz-juelich.de)

Abstract. Water vapour convectively injected into the mid-latitude lowermost stratosphere could affect stratospheric ozone. The associated potential ozone loss process requires low temperatures and an elevated water vapour mixing ratio. An increase in sulphate aerosol surface area due to a volcanic eruption or geoengineering could increase the likelihood of occurrence of this process. However, the chemical mechanism of this ozone loss process has not yet been analysed in sufficient detail and its sensitivity to various conditions is not yet clear. Under conditions of climate change associated with an increase in greenhouse gases, both a stratospheric cooling and an increase in water vapour convectively injected into the stratosphere is expected. Understanding the influence of low temperatures, elevated water vapour and enhanced sulphate particles on this ozone loss mechanism is a key step in estimating the impact of climate change and potential sulphate geoengineering on mid-latitude ozone.

Here, we analyse the ozone loss mechanism and its sensitivity to various stratospheric conditions in detail. Conducting a box-model study with the Chemical Lagrangian Model of the Stratosphere (CLaMS), chemistry was simulated along a 7-day backward trajectory. This trajectory was calculated neglecting mixing of neighbouring air masses. Chemical simulations were initialized using measurements taken during the Study of Emissions and atmospheric Composition, Clouds and Climate Coupling by Regional Surveys (SEAC^{4}RS) aircraft campaign (2013, Texas), which encountered an elevated water vapour mixing ratio at a pressure level around 100 hPa. We present a detailed analysis of the ozone loss mechanism, including the chlorine activation, chlorine catalysed ozone loss cycles, maintenance of activated chlorine and the role of active nitrogen oxide radicals (NO_x). Focussing on a realistic trajectory in a temperature range from 197–203 K, a threshold in water vapour of 11.0–11.6 ppmv has to be exceeded and maintained for stratospheric ozone loss to occur. We investigated the sensitivity of the water vapour threshold to temperature, sulphate content, inorganic chlorine (Cl_y), inorganic nitrogen (NO_y) and inorganic bromine (Br_y). The water vapour threshold is mainly determined by the temperature and sulphate content. However, the amount of ozone loss depends on Cl_y, NO_y, Br_y and the duration of the time period over which chlorine activation can be maintained. Our results show that to deplete ozone, a chlorine activation time of 24 to 36 hours for conditions of the water vapour threshold with low temperatures and high water vapour mixing ratios must be maintained. A maximum ozone loss of 9% was found for a 20 ppmv water vapour mixing ratio at North American Monsoon (NAM) tropopause standard conditions with the model run

Atmos. Chem. Phys. Discuss., https://doi.org/10.5194/acp-2018-1193
Manuscript under review for journal Atmos. Chem. Phys.
Discussion started: 12 December 2018

Atmospheric Chemistry and Physics Discussions

along a realistic trajectory. For the same trajectory, using observed conditions (of 10.6 ppmv), whether ozone loss occurs was simulated dependent on the sulphate amount assumed. Detailed analysis of current and future possibilities is needed to assess whether enhanced water vapour conditions in the summertime mid-latitude lower stratosphere leads to significant ozone loss.

1 Introduction

The impact of water vapour convectively injected into the lowermost stratosphere on the mid-latitude ozone layer is a matter of current debate (Anderson et al., 2012, 2017; Ravishankara, 2012; Schwartz et al., 2013). Borrmann et al. (1996, 1997) and Solomon et al. (1997) investigated the influence of cirrus clouds on ozone chemistry in the lowermost stratosphere. Anderson et al. (2012) proposed a potential ozone depletion in the mid-latitude stratosphere in summer under conditions of enhanced water vapour and low temperatures. They proposed chemical ozone loss to occur under these conditions through processes related to ozone loss known from polar regions early spring (e.g. Grooß et al., 2011; Solomon, 1999; Vogel et al., 2011). Here, we present a detailed analysis of this ozone loss mechanism and an extensive investigation of its sensitivity to a variety of conditions.

In the bulk and on the surface of cold condensed stratospheric particles, such as binary H_2SO_4/H_2O solutions, ternary solutions, NAT (Nitric Acid Trihydrate) and ice particles (e.g. Spang et al., 2018), inactive chlorine species (HCl, $ClONO_2$) can be converted to active chlorine (ClO_x=Cl+ClO+2 $\times$ Cl_2O_2) through the heterogeneous reactions R1, R2 and R3 (Solomon et al., 1986; Prather, 1992; Crutzen et al., 1992) and the subsequent photolysis of Cl_2 and HOCl.

$$ClONO_2 + HCl \rightarrow HNO_3 + Cl_2 \quad \text{(R1)}$$

$$ClONO_2 + H_2O \rightarrow HNO_3 + HOCl \quad \text{(R2)}$$

$$HCl + HOCl \rightarrow H_2O + Cl_2 \quad \text{(R3)}$$

The heterogeneous reactions R1 and R2 drive the conversion of active nitrogen-oxides (NO_x) into HNO_3. After chlorine activation, catalytic ozone loss cycles can occur, such as the ClO-dimer-cycle (Molina and Molina, 1987, **C1**) and the ClO-BrO-cycle (McElroy et al., 1986, **C2**). These cycles are responsible for the rapid ozone loss observed in Antarctic spring (e.g. Solomon, 1999).

ClO-Dimer-Cycle (**C1**):

$$ClO + ClO + M \rightarrow ClOOCl + M \quad \text{(R4)}$$

$$ClOOCl + h\nu \rightarrow Cl + ClOO \quad \text{(R5)}$$

$$ClOO + M \rightarrow Cl + O_2 + M \quad \text{(R6)}$$

$$2x(Cl + O_3 \rightarrow ClO + O_2) \quad \text{(R7)}$$

$$\text{net: } 2O_3 + h\nu \rightarrow 3O_2 \quad \textbf{(C1)}$$

Atmos. Chem. Phys. Discuss., https://doi.org/10.5194/acp-2018-1193
Manuscript under review for journal Atmos. Chem. Phys.
Discussion started: 12 December 2018

Atmospheric Chemistry and Physics Discussions

ClO-BrO-Cycle (**C2**):

$$\mathrm{ClO} + \mathrm{BrO} \rightarrow \mathrm{Br} + \mathrm{Cl} + \mathrm{O_2} \quad \text{(R8)}$$

$$\mathrm{Br} + \mathrm{O_3} \rightarrow \mathrm{BrO} + \mathrm{O_2} \quad \text{(R9)}$$

$$\mathrm{Cl} + \mathrm{O_3} \rightarrow \mathrm{ClO} + \mathrm{O_2} \quad \text{(R7)}$$

$$\text{net: } 2\,\mathrm{O_3} \rightarrow 3\,\mathrm{O_2} \quad \textbf{(C2)}$$

In a third catalytic ozone loss cycle, **C3**, HOCl is formed and subsequently photolysed yielding OH and Cl radicals leading to stratospheric ozone destruction. This cycle was originally proposed by Solomon et al. (1986) as an ozone depleting cycle in the Antarctic lower stratosphere, but for polar ozone destruction, this cycle turned out to be of minor importance (Solomon, 1999). Nevertheless, **C3** would be expected to play a role in ozone loss in the mid-latitude lower stratosphere (e.g. Daniel et al., 1999; Ward and Rowley, 2016).

$$\mathrm{ClO} + \mathrm{HO_2} \rightarrow \mathrm{HOCl} + \mathrm{O_2} \quad \text{(R10)}$$

$$\mathrm{HOCl} + \mathrm{h}\nu \rightarrow \mathrm{Cl} + \mathrm{OH} \quad \text{(R11)}$$

$$\mathrm{OH} + \mathrm{O_3} \rightarrow \mathrm{HO_2} + \mathrm{O_2} \quad \text{(R12)}$$

$$\mathrm{Cl} + \mathrm{O_3} \rightarrow \mathrm{ClO} + \mathrm{O_2} \quad \text{(R7)}$$

$$\text{net: } 2\,\mathrm{O_3} + \mathrm{h}\nu \rightarrow 3\,\mathrm{O_2} \quad \textbf{(C3)}$$

Under the very dry conditions in the polar stratosphere, very low temperatures (below ∼195 K) are required for heterogeneous chlorine activation through reactions R1–R3 (Solomon, 1999; Shi et al., 2001). An enhancement of water vapour above background values would allow chlorine activation at higher temperatures (200–205 K) (Drdla and Müller, 2012), which led to the hypothesis hat chlorine activation and subsequent ozone loss could occur at mid-latitudes in summer in the lowermost stratosphere (Anderson et al., 2012, 2017; Anderson and Clapp, 2018).

An enhanced stratospheric sulphate aerosol content increases heterogeneous chlorine activation by increasing the surface area of the condensed particles (Drdla and Müller, 2012; Solomon, 1999). As an example, the aerosol surface area density in the lower stratosphere ranges between ∼0.5 and 1.5 $\mu\mathrm{m^2cm^{-3}}$ under non-volcanic conditions (Thomason and Peter, 2006), while the perturbation of Mt. Pinatubo yielded peak values of more than 40 $\mu\mathrm{m^2cm^{-3}}$ (Thomason et al., 1997). In the stratosphere, water vapour increases with altitude, primarily due to methane oxidation (LeTexier et al., 1988; Rohs et al., 2006). The upper branch of the Brewer Dobson circulation (BDC) transports higher stratospheric water vapour mixing ratios down to lower altitudes at mid to high latitudes, and this air mixes with the low water vapour containing air from the tropics that has moved poleward in the lower branch of the BDC (e.g. Brewer, 1949; Randel et al., 2004; Schwartz et al., 2013; Konopka et al., 2015; Poshyvailo et al., 2018), giving typical mid-latitude lowermost stratosphere values of 2–6 ppmv $\mathrm{H_2O}$.

However, above North America in summer enhanced water vapour mixing ratios of 10–18 ppmv at an altitude of ∼16.5 km (380 K potential temperature, ∼ 100 hPa) (Smith et al., 2017) have been observed, which were connected with deep convective

Atmos. Chem. Phys. Discuss., https://doi.org/10.5194/acp-2018-1193
Manuscript under review for journal Atmos. Chem. Phys.
Discussion started: 12 December 2018

storm systems penetrating the tropopause (Homeyer et al., 2014; Herman et al., 2017; Smith et al., 2017). These convective overshooting events can transport ice crystals into the lowermost stratosphere, where the ice evaporates leading to a local enhancement of water vapour (Hanisco et al., 2007; Schiller et al., 2009; Herman et al., 2017).

As greenhouse gases increase, models predict that more water may be convectively transported into the stratosphere (Trapp et al., 2009; Klooster and Roebber, 2009). This increases the possibility that the ozone loss process proposed by Anderson et al. (2012) will occur, especially in the case of an additional enhancement of stratospheric sulphate particles caused by volcanic eruptions or sulphate geoengineering. However, the occurrence of this ozone loss process requires halogens to be present, which are decreasing in the stratosphere due to the Montreal Protocol ans its amendments and adjustments (WMO, 2014). For estimating the impact of both climate change and a possible sulphate geoengineering on the mid-latitude ozone layer, it is necessary to consider the influence of enhanced water vapour and sulphate content on mid-latitude ozone chemistry in the lowermost stratosphere in more detail.

In the study by Anderson et al. (2012), a range of initial mixing ratios for HCl and $ClONO_2$ with rather high concentrations of 850 pptv HCl and 150 pptv $ClONO_2$ was assumed. Here, we investigate ozone loss in mid-latitude summer based on measurements from flights by the NASA ER-2 aircraft during the Studies of Emissions and Atmospheric Composition, Clouds and Climate Coupling by Regional Surveys (SEAC^{4}RS) campaign, which was based in Houston, Texas in 2013 (Toon et al., 2016). Conducting box-model simulations with the Chemical Lagrangian Model of the Stratosphere (CLaMS, McKenna et al., 2002a, b), the ozone loss mechanism is analysed in greater detail. The model setup is described in Section 2. In Sec. 3, the chlorine activation step, catalytic ozone loss cycles and the maintenance of activated chlorine levels in the mid-latitude stratosphere are investigated in detail. The sensitivity of this mechanism to water vapour, sulphate content, temperature, Cl_y mixing ratio (Cl_y=HCl+$ClONO_2$+ClO_x), reactive nitrogen (NO_y=NO_x+HNO_3 $2N_2O_5$+NO_3) and inorganic bromine (Br_y) is explored in Sec. 4. Case studies, which extend the simulated time period and assume conditions based on both SEAC^{4}RS and MACPEX (Mid-latitude Airborne Cirrus Properties Experiment) measurements as well as conditions used in the study of Anderson et al. (2012) further illustrate these sensitivities in Sec. 5.

2 Model setup

The simulations presented here were performed with the box-model version of CLaMS (McKenna et al., 2002a, b). Stratospheric chemistry is simulated based on a setup used in previous studies (Grooß et al., 2011; Müller et al., 2018; Zafar et al., 2018) for single air parcels along trajectories including diabatic descent and neglecting mixing between neighbouring air masses. A full chemical reaction scheme comprising gas phase and heterogeneous chemistry is applied using the SVODE-solver (Brown et al., 1989). Chemical reaction kinetics are taken from Sander et al. (2011), heterogeneous reaction rates for R1–R3 were calculated based on the the study of Shi et al. (2001), and photolysis rates are calculated for spherical geometry (Becker et al., 2000). In contrast to the setup in Grooß et al. (2011), Müller et al. (2018) and Zafar et al. (2018), only formation of liquid particles (both binary H_2O/H_2SO_4 and ternary $HNO_3/H_2O/H_2SO_4$ solutions) is allowed (i.e. no NAT or ice particles

Atmos. Chem. Phys. Discuss., https://doi.org/10.5194/acp-2018-1193
Manuscript under review for journal Atmos. Chem. Phys.
Discussion started: 12 December 2018

are formed in this model setup). Note that this is also different from the study of and to the study of Borrmann et al. (1996, 1997), who investigated lowermost stratospheric ozone chemistry on cirrus clouds.

2.1 Measurements

The box model simulations were initialized using water vapour, ozone and CH_4 measurements taken during the SEAC^{4}RS aircraft campaign and water vapour, ozone and N_2O measurements taken during MACPEX campaign (more information on the chemical initialization is provided in Section 2.3). The investigation of mid-latitude ozone chemistry presented here is primarily based on SEAC^{4}RS conditions, while simulations based on MACPEX data were conducted to complement the results of the investigation by showing a further measurement-based example. The SEAC^{4}RS campaign took place during the North American summertime, while the MACPEX campaign was in spring, prior to the build up of the North American Monsoon (NAM) anticyclone.

The SEAC^{4}RS campaign was based in Houston, Texas, and took place during August and September 2013 (Toon et al., 2016). One aim of this campaign was to investigate the impact of deep convective clouds on the water vapour content and the chemistry in the lowermost stratosphere. We initialized the model using measurements taken on 8 August 2013 by the Harvard Lyman-a photofragment fluorescence hygrometer (HWV, Weinstock et al., 2009), which flew on the NASA ER-2 high altitude research aircraft. Ozone was initialized in our simulations, using O_3 measurements from the National Oceanic and Atmospheric Administration (NOAA) UAS-O_3-instrument (Gao et al., 2012). Initial Cl_y and NO_y were determined using tracer-tracer correlations (for more informations see Sec. 2.3) based on methane measurements with the Harvard University Picarro Cavity Ring down Spectrometer (HUPCRS) (Werner et al., 2017).

The simulation results initialized with SEAC^{4}RS measurements were compared with a case of enhanced lower stratospheric water sampled during the spring 2011 MACPEX campaign (Rollins et al., 2014) also based in Houston, Texas. The water vapour values used here were measured by the Fast In-situ Stratospheric Hygrometer (FISH), which employs the Lyman-α photofragment fluorescence technique (Meyer et al., 2015). MACPEX ozone was measured by the UAS-O_3 instrument (Gao et al., 2012). Initial Cl_y and NO_y were assumed based on tracer-tracer correlations with N_2O that was measured by the Jet Propulsion Laboratory's Aircraft Laser Infrared Absorption Spectrometer (ALIAS) instrument (Webster et al., 1994).

2.2 Trajectories

Diabatic trajectories were calculated using wind and temperature data from the ERA-Interim reanalysis (Dee et al., 2011) with $1^\circ \times 1^\circ$ resolution provided by the European Centre for Medium-Range Weather Forecasts (ECMWF). The vertical velocities were calculated from the total diabatic heating rates derived from ERA-Interim data (Ploeger et al., 2010). Trajectories (7 day forward and backward) were initialized at locations during MACPEX and SEAC^{4}RS where stratospheric water vapour was over 10 ppmv.

Selected examples of calculated trajectories are shown in Fig. 1. These trajectories were chosen for the chemical analysis, because their initial conditions exhibited enhanced water vapour relative to the overall background and the temperatures were very low. These are then the most suitable for the occurrence of the mechanism proposed by Anderson et al. (2012). In the left

panel, backward trajectories are presented in the range of −7 to 0 days from the time of measurement and forward trajectories in the range from 0 to 7 days. In the right panel, the location of the measurement is shown by a red square. The black trajectory refers to a measurement on 11 April 2011 during the MACPEX campaign. The potential temperature level of this trajectory is around 380 K and above the tropopause located at ∼350 K, which was deduced from the temperature profile measured during the flight on 11 April 2011. The backward trajectory reaches very low temperatures with a minimum temperature of 191 K. The forward trajectory shows a strongly increasing temperature and pressure level due to a decrease in altitude. Coming from the Western Pacific, this air parcel passes the North American continent briefly. For this study numerous water measurements of the MACPEX campaign were analysed, but only few values of more than 10 ppmv were observed above the tropopause.

The trajectory marked in blue in Fig. 1 is based on measurements on 8 August 2013 during the SEAC^{4}RS campaign. With a potential temperature of 380 to 390 K, this trajectory is above the tropopause of ∼370 K, deduced from the temperature profile measured during the flight. Both, the forward and backward trajectories stay in the region of the North American continent. For the SEAC^{4}RS campaign, the temperature range of the backward trajectory varies between 197 and 202 K and the forward trajectory exhibits increasing temperatures. In addition, we considered trajectories based on other SEAC^{4}RS measurements with enhanced water vapour, however most of them exhibit higher mean temperatures of at least 200 K. Since low temperatures are expected to push stratospheric ozone depletion in mid-latitudes (Anderson et al., 2012) due to faster heterogeneous chemical reactions and thus faster chlorine activation, the SEAC^{4}RS backward trajectory (Fig.1, blue, day −7 to 0) is selected here as the standard trajectory. This trajectory is used to analyse the chemical mechanisms affecting lower stratospheric ozone under various water vapour conditions, and to explore the sensitivity of these processes to different initial conditions.

2.3 Initialization

Important trace gases for ozone chemistry – O_3, Cl_y and NO_y – are initialized based on measurements during the SEAC^{4}RS and MACPEX aircraft campaigns over North America (see Sec. 2.1). Ozone and water vapour were measured directly during the aircraft campaigns, Cl_y and NO_y are inferred from tracer-tracer relations using either CH_4 (SEAC^{4}RS) or N_2O (MACPEX) measured on the aircraft employed. The initialization of all further trace gases except of water vapour were taken from the full chemistry 3D-CLaMS simulation (Vogel et al., 2015, 2016) for summer 2012 at the location of the measurement. Chemistry was initialized 7 days before the measurement. However, this time shift does not affect the sensitivities and the mechanism investigated here, because the trace gases Cl_y and NO_y were initialized based on measured CH_4 and N_2O mixing ratios, which are not significantly changing during a 7-day box-model simulation.

2.3.1 Standard case

In the standard case, the initial values of O_3, Cl_y and NO_y are determined based on an observation with an enhanced water vapour content of 10.6 ppmv (measured by the HWV-instrument) from the SEAC^{4}RS (Toon et al., 2016) aircraft campaign. A gas phase equivalent mixing ratio for background sulphuric acid (H_2SO_4) of 0.20 ppbv is assumed. Initial CO (49.6 ppbv) is taken from the 3D-CLaMS simulation (Vogel et al., 2015), which is higher than the measured value of 34.74 ppbv (measured by the HUPCRS instrument). Simulations assuming the measured CO mixing ratio showed only a minor difference to the

Atmos. Chem. Phys. Discuss., https://doi.org/10.5194/acp-2018-1193
Manuscript under review for journal Atmos. Chem. Phys.
Discussion started: 12 December 2018

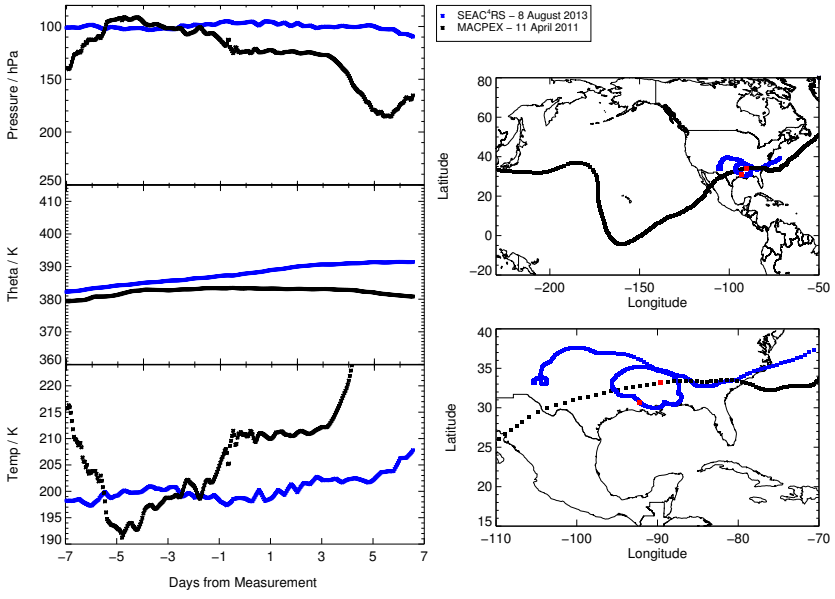

Figure 1. Pressure, potential temperature, temperature and location of selected trajectories calculated based on measurements with enhanced water vapour during the MACPEX (black) and SEAC^{4}RS (blue) aircraft campaigns. Red squares mark the location of the measurement (right). For the right panels the bottom panel exhibits a zoom from the top panel. In the bottom panel, the MACPEX trajectory consists of single squares due to a faster movement of the air parcel in that region.

results presented here. The initial values for the main trace gases for the standard case are summarized in Table 1. Note, in the 3D-CLaMS simulation, the mixing ratios of HCl (131 ppt, CLaMS), O_3 (206 ppb, CLaMS) and HNO_3 (354 ppt, CLaMS) are at the location of the SEAC^{4}RS measurement lower than in the standard initialization (see Tab. 1).

Since Cl_y and NO_y were not measured during the SEAC^{4}RS ER2-flights in the lowermost stratosphere, values for Cl_y and NO_y are calculated through tracer-tracer correlations (Grooß et al., 2014, see Appendix A for equations) based on a SEAC^{4}RS CH_4 measurement (of 1.776 ppmv) on 8 August 2013. The Cl_y-CH_4 correlation was calculated from measurements of the Airborne Chromatograph for Atmospheric Trace Species (ACATS) during flights of the ER-2 aircraft and from measurements by the cryogenic whole air sampler (Triple) during balloon flights at mid and high latitudes in the year 2000 (Grooß et al., 2002). Between the year 2000 and 2013 stratospheric CH_4 increased and Cl_y decreased. Hence, the change of both lowermost stratospheric CH_4 and Cl_y has to be taken into account when using this tracer-tracer correlation. The increase in CH_4 was estimated to be equivalent to the growth rate for tropospheric CH_4. This growth rate was calculated to be 45.8 ppb from the year 2000 to 2013 by determining and adding every annual mean of the tropospheric CH_4 growth rate given in GHG Bulletin (2014). Subtracting this increase of CH_4 from the measured CH_4 mixing ratio yields an equivalent-CH_4 for the year 2000. From the CH_4 equivalent, an equivalent Cl_y mixing ratio for the year 2000 was calculated using the tracer-tracer correlation (Grooß et al., 2014). The annual decrease of Cl_y is assumed to be 0.8% (WMO, 2014) from the year 2000 to 2013, and thus

Atmos. Chem. Phys. Discuss., https://doi.org/10.5194/acp-2018-1193
Manuscript under review for journal Atmos. Chem. Phys.
Discussion started: 12 December 2018

Atmospheric Chemistry and Physics Discussions

the initial Cl_y is calculated to be 156 ppt.

Initial NO_y was calculated through a N_2O correlation. Since no N_2O was measured on the ER2-flights during SEAC^{4}RS, stratospheric N2O was first estimated through a methane correlation (Grooß et al., 2002), which is based on measurements from the year 2000. Hence, the equivalent CH_4 mixing ratio for the year 2000 (see above) was used to calculate an N_2O equivalent. Considering an estimated increase in N_2O of 10.4 ppb from 2000 to 2013, which was determined in the same way as the CH_4 change (GHG Bulletin, 2014), the N_2O mixing ratio related to the time of the measurement in 2013 was calculated. Afterwards NO_y is calculated with a correlation from Grooß et al. (2014) to be 782.9 ppt.

This standard case initialization is shown in Table 1. Because of the uncertain conditions in convective overshooting plumes, sensitivity box-model simulations are conducted. Furthermore, testing the impact of various parameters on chemical ozone loss is intended to yield a better understanding of the balance between stratospheric ozone production and ozone loss, which is a key aspect for potential mid-latitude ozone depletion. The assumed water vapour content in a simulation is varied from 5 to 20 ppmv. In addition, simulations assuming the same water vapour range and a constant temperature in a range from 195–220 K are conducted assuming sulphate background conditions with a gas phase equivalent of 0.20 ppbv and 10×enhanced sulphate (2.00 ppbv) for illustrating the dependence of ozone loss on water vapour and temperature. Furthermore, sensitivity simulations are conducted, assuming 80% Cl_y, 80% NO_y or 50% Br_y, and a standard case simulation along a 19-day trajectory is calculated.

Table 1. Mixing ratios and sources used for initialization of relevant trace gases. The standard initialization is based on SEAC^{4}RS measurements. Cl_y and NO_y values were determined based on tracer-tracer correlations (see text) for the standard and the MACPEX case. The high Cl_y case is based on Fig. 2 from Anderson et al. (2012). Initial mixing ratios of ClO_x species were assumed to be zero for all cases.

	Standard case			Case of high Cl_y		MACPEX case	
Species	Value	Source	Sensitivity simulation	Value	Source	Value	Source
O_3	303.2 ppbv	UAS-O_3		303.2 ppbv	UAS-O_3	283.0 ppbv	UAS-O_3
CH_4	1.76 ppmv	CLaMS-3D		1.76 ppmv	CLaMS-3D	1.68 ppmv	CLaMS-3D
CO	49.6 ppbv	CLaMS-3D		49.6 ppbv	CLaMS-3D	19.0 ppbv	CLaMS-3D
HCl	149.5 pptv	tracer corr.	80% Cl_y	850 pptv	Anderson et al. (2012)	52.7 pptv	tracer corr.
$ClONO_2$	6.2 pptv	tracer corr.		150 pptv	Anderson et al. (2012)	2.19 pptv	tracer corr.
HNO_3	439.23 pptv	tracer corr.	80% NO_y	1.19 ppbv	see section 2.3.2	390.3 pptv	tracer corr.
NO	144.8 pptv	tracer corr.		325 pptv	Anderson et al. (2012)	114.6 pptv	tracer corr.
NO_2	144.8 pptv	tracer corr.		375 pptv	Anderson et al. (2012)	114.6 pptv	tracer corr.
Br_y	6.9 pptv	CLaMS-3D	50% Br_y	6.9 pptv	CLaMS-3D	1.2 pptv	CLaMS-3D
H_2O	5–20 ppmv		5–20 ppmv	5–20 ppmv		5–20 ppmv	
H_2SO_4	0.2 ppbv, 0.6 ppbv, 2.0 ppbv			0.2 ppbv, 0.6 ppbv		0.2 ppbv, 0.6 ppbv	
Temperature	195–220 K		const. temp				

Atmos. Chem. Phys. Discuss., https://doi.org/10.5194/acp-2018-1193
Manuscript under review for journal Atmos. Chem. Phys.
Discussion started: 12 December 2018

2.3.2 Case of high Cl_y

Simulations conducted assuming high Cl_y and NO_y concentrations taken from Fig. 2 in Anderson et al. (2012) are referred to as "Case of high Cl_y", which constitutes a worst case scenario. In the case of high Cl_y, HNO_3 is determined as 1.19 ppb assuming the same ratio for HNO_3 (63% of total NO_y) and NO+NO_2 (37% of total NO_y) as in the standard case. An overview of the important trace gases in the initialization is given in Tab. 1. The results of the case initialize with high Cl_y are compared with the results obtained from standard case simulations.

2.3.3 MACPEX Case

Similar to the standard case, a simulation based on measurements during the MACPEX aircraft campaign 2011 (Rollins et al., 2014) was conducted, referred to as "MACPEX Case". This case presents a further example for an event with high stratospheric water vapour based on airborne measurements and complements the results obtained from the standard case. All trace gases except for ozone, Cl_y, NO_y and water vapour are taken from a 3D-CLaMS-simulation (Vogel et al., 2015, 2016). Initial Cl_y and NO_y is calculated based on N_2O and CH_4 tracer-tracer correlations (Grooß et al., 2014) with corrections considering a N_2O increase from 2009 to 2013 and a CH_4 increase from 2000 to 2009. Cl_y is determined using the same correlation with CH_4 as for the standard case. Therefore CH_4 is first calculated using measured N_2O of 320.28 ppbv and a correlation based on measurements from 2009 (Grooß et al., 2014). The increase of stratospheric CH_4 and N_2O is considered as described for the standard case (GHG Bulletin, 2014). First, an increase in N_2O of 1.6 ppb from 2009 to 2011 is estimated to adjust N_2O. Furthermore calculated CH_4 is adjusted considering a difference between CH_4 in 2000 and 2009 of 0.026 ppm. The annual decrease of Cl_y from 2000 to 2011 is assumed to be 0.8% (WMO, 2014). A summary of the initial values for main tracers assumed in the MACPEX case are given in Table 1.

3 Mid-latitude ozone chemistry

Mid-latitude ozone chemistry in the lowermost stratosphere depends on water vapour abundance and temperature. This study focuses on the water vapour dependence of stratospheric ozone chemistry by analysing chemical processes occurring in a box-model simulation along a realistic trajectory in the temperature range from 197-203 K under several water vapour conditions. In Figure 2 the mixing ratio of ozone, ClO_x and NO_x is shown for two simulations assuming 5 ppmv (dashed line) and 15 ppmv (solid line) H_2O. For the low water vapour (5 ppmv) case, net ozone formation occurs, the ClO_x mixing ratio remains low and the NO_x mixing ratio high. In contrast, assuming a water vapour mixing ratio of 15 ppmv, ozone depletion accompanied by a decrease in NO_x occurs, coupled with chlorine activation as indicated by the increasing ClOx mixing ratio. The sensitivity to variations in water vapour conditions on stratospheric ozone is tested here by conducting simulations with standard conditions but varying the assumed water vapour mixing ratio from 5 to 20 ppmv in varying increments, with the resolution increased near the changeover from ozone production to destruction.

Atmos. Chem. Phys. Discuss., https://doi.org/10.5194/acp-2018-1193
Manuscript under review for journal Atmos. Chem. Phys.
Discussion started: 12 December 2018

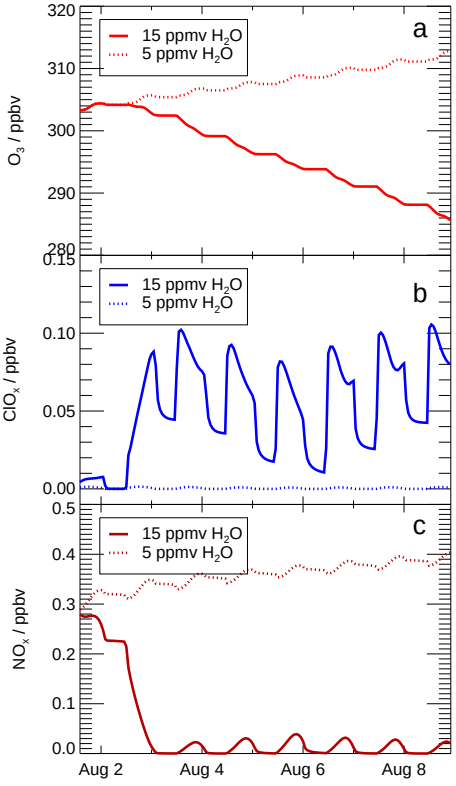

Figure 2. Volume mixing ratio of O_3 (panel a), ClO_x (panel b) and NO_x (panel c) during a simulation with 15 ppmv H_2O and 5 ppmv H_2O.

In Figure 3, the ozone values reached at the end of the 7-day simulation (end ozone, blue squares) are plotted as a function of the assumed water vapour mixing ratio. The initial ozone value, of 303.2 ppbv, is shown by the grey line. Blue squares lying above that line are cases with ozone production, those lying below that line are cases with ozone destruction. The threshold is determined as the water vapour mixing ratio at which the end ozone value clearly falls below the end ozone that is reached for low water vapour amounts. For the standard case shown in Fig. 3, this threshold is reached at a water vapour mixing ratio in the range of 11.0 to 11.6 ppmv. By 12 ppmv of water vapour, the system is clearly in an ozone destruction regime. The occurrence of the water vapour threshold and ozone depletion is related to chlorine activation. The time until chlorine activation occurs in the simulation is plotted in Fig. 3 as violet triangles. Assuming that chlorine activation occurs when the ClO_x mixing ratio exceeds 10% of total Cl_y (Drdla and Müller, 2012), plotted here is the time when chlorine activation first occurs in the model. Since the ClO_x/Cl_y ratio is dependent on the diurnal cycle, the 24-hours mean value of the ClO_x mixing ratio was used to determine the chlorine activation time. For low water vapour mixing ratios, no chlorine activation time is plotted, because no chlorine activation occurs. Chlorine activation only occurs when the water vapour threshold is exceeded (Fig. 3). Near the water

Atmos. Chem. Phys. Discuss., https://doi.org/10.5194/acp-2018-1193
Manuscript under review for journal Atmos. Chem. Phys.
Discussion started: 12 December 2018

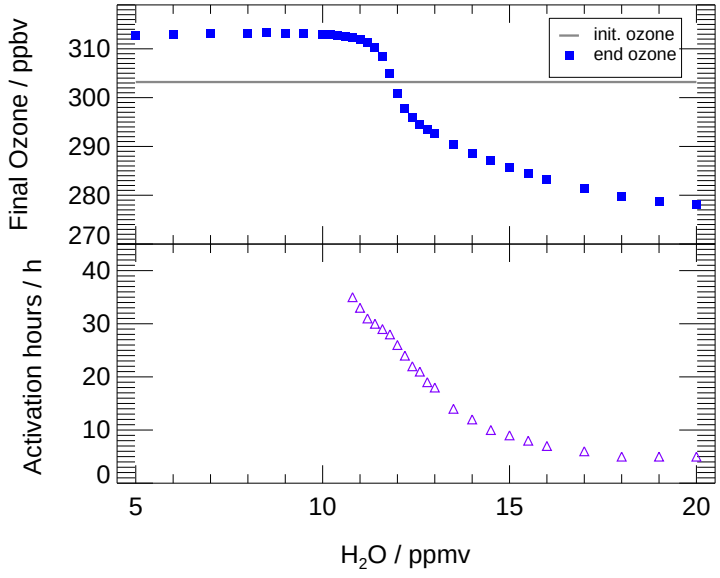

Figure 3. Impact of the water vapour content on the ozone mixing ratio (final ozone, blue squares) reached at the end of the 7-day simulation along the standard trajectory and assuming standard conditions. The initial ozone amount is marked by the grey line. In the bottom panel, violet triangles show the time until chlorine activation occurs is. For low water vapour mixing ratios no chlorine activation occurs.

vapour threshold, the activation time is 24 to 36 hours and it decreases with increasing water vapour mixing ratios. It requires 5 hours at 20 ppmv H_2O. The shorter the chlorine activation time, the longer activated chlorine exists during the simulation yielding greater ozone depletion. The processes yielding ozone depletion at high water vapour conditions as well as ozone formation at low water vapour are analysed in detail in the subsequent sections. For this investigation we use the simulated reaction rates for each chemical reaction along the course of the calculation. For high water vapour mixing ratios the roles of both chlorine activation and a decrease in the NO_x mixing ratio (Fig. 2) are discussed.

3.1 Ozone formation at low water vapour mixing ratios

At water vapour mixing ratios up to 11.8 ppmv, ozone formation occurs (see Fig. 3). This ozone formation is mainly driven by the photolysis of O_2

$$O_2 + h\nu \rightarrow 2\,O(^3P) \qquad \text{(R13)}$$

and the subsequent reaction

$$O_2 + O(^3P) + M \rightarrow O_3 + M. \qquad \text{(R14)}$$

Atmos. Chem. Phys. Discuss., https://doi.org/10.5194/acp-2018-1193
Manuscript under review for journal Atmos. Chem. Phys.
Discussion started: 12 December 2018

Atmospheric Chemistry and Physics Discussions

Additionally, photolysis of NO_2

$$NO_2 + h\nu \rightarrow NO + O(^3P) \quad \text{(R15)}$$

followed by R14 leads to ozone formation. NO radicals, which are formed in R15, mainly react with ozone as well as ClO and BrO forming Cl and Br radicals.

$$NO + O_3 \rightarrow O_2 + NO_2 \quad \text{(R16)}$$

$$ClO + NO \rightarrow Cl + NO_2 \quad \text{(R17)}$$

$$BrO + NO \rightarrow Br + NO_2 \quad \text{(R18)}$$

Since these radicals react with ozone in reaction R7 ($Cl + O_3$) and R9 ($Br + O_3$), not all of the $O(^3P)$ formed in R15 yields a net ozone formation. However, R15 is part of the "Ozone Smog Cycle" (Haagen-Smit, 1952) known from tropospheric chemistry, which has also an impact on stratospheric chemistry (Grenfell et al., 2006; Grooß et al., 2011).

$$OH + CO \rightarrow CO_2 + H \quad \text{(R19)}$$

$$H + O_2 + M \rightarrow HO_2 + M \quad \text{(R20)}$$

$$HO_2 + NO \rightarrow NO_2 + OH \quad \text{(R21)}$$

$$NO_2 + h\nu \rightarrow NO + O(^3P) \quad \text{(R15)}$$

$$O_2 + O(^3P) + M \rightarrow O_3 + M \quad \text{(R14)}$$

$$\text{net: } CO + 2\,O_2 \rightarrow CO_2 + O_3 \quad \textbf{(C4)}$$

The rate of this cycle is determined by reaction R19 at low water vapour mixing ratios, and its net reaction is the oxidation of CO. The ozone formation through this cycle contributes around 40% to the total ozone formation at 5 ppmv in our box model standard simulation. Hence, the ozone formation which occurs in the simulations assuming low water vapour mixing ratios is due to both the photolysis of O_2 and cycle **C4**.

3.2 Ozone loss at high water vapour mixing ratios

For higher water vapour mixing ratios than 11 ppmv, ozone depletion is simulated (Fig. 3). The ozone loss mechanism generally consists of two steps: a chlorine activation step transferring inactive chlorine (HCl) into active ClO_x followed by catalytic ozone loss processes (Anderson et al., 2012). We analyse both the chlorine activation step and subsequent catalytic ozone loss cycles potentially occurring in mid-latitudes in the lower stratosphere under enhanced water vapour conditions. Since ozone depletion is larger at high water vapour mixing ratios, conditions with a water vapour mixing ratio of 15 ppmv are chosen here to analyse the chemical ozone loss mechanism. Figure 4 shows an overview of the development of important mixing ratios and reaction rates during the 7-day simulation. Panel a illustrates temperature (black line) and surface area density of liquid particles (blue line).

The first phase of the ozone loss mechanism (dark grey background in Fig. 4) is dominated by the occurrence of heterogeneous

Atmos. Chem. Phys. Discuss., https://doi.org/10.5194/acp-2018-1193
Manuscript under review for journal Atmos. Chem. Phys.
Discussion started: 12 December 2018

reactions. The most important heterogeneous chlorine activation reaction is R1 (Fig. 4b), which leads to the chlorine activation chain (von Hobe et al., 2011)

$$ClO + NO_2 + M \rightarrow ClONO_2 + M \quad (R22)$$

$$ClONO_2 + HCl \rightarrow Cl_2 + HNO_3 \quad (R1)$$

$$Cl_2 + h\nu \rightarrow 2Cl \quad (R23)$$

$$2 \times (Cl + O_3 \rightarrow ClO + O_2) \quad (R7)$$

net: $HCl + NO_2 + 2O_3 \rightarrow ClO + HNO_3 + 2O_2$.

This chlorine activation chain yields a transformation of inactive HCl into active ClO_x as well as of NO_x into HNO_3. The ozone loss due to this reaction chain is negligible and no depleting effect on ozone occurs during the first phase (Fig. 4c). In Fig. 4g, the NO_x mixing ratio is seen to decrease and HNO_3 increases due R1. Further, in the first phase the HCl mixing ratio decreases, yielding an increase of ClO_x (Fig. 4f). The delay between HCl reduction and ClO_x formation (Fig. 4f) is caused by the combination of the diurnal cycle and the accumulation of Cl_2 and Cl_2O_2 during night. Both decreasing NO_x and increasing ClO_x have an impact on ozone during the second phase of the ozone loss mechanism (light grey background in Fig. 4), which is characterized by a decreasing ozone mixing ratio (Fig. 4c). The role of NO_x and ClO_x is discussed in detail in the next sections.

3.2.1 Role of NO_x

The transformation of NO_x-radicals into HNO_3 is due to R22 ($ClO+NO_2$) and subsequent the occurrence of the heterogeneous reactions R1 ($ClONO_2 + HCl$) and R2 ($ClONO_2 + H_2O$), which form HNO_3. This behaviour was also found in former studies (e.g. Keim et al., 1996; Pitari et al., 2016; Berthet et al., 2017), investigating the impact of volcanic aerosols on stratospheric ozone chemistry. Dependent on temperature and water vapour content, the HNO_3 formed is taken up into condensed particles. In the standard simulation using 15 ppmv H_2O, an uptake of 64% is reached on the day with the lowest temperature (197.3 K, 2 Aug 2013), while at higher temperatures (4–7 August 2013) 85% of HNO_3 remain in the gas phase. After the transformation of NO_x into HNO_3, the NO_x mixing ratio remains low in the second phase of the mechanism (Fig. 4d, light grey region) while the HNO_3 mixing ratio (cond.+gas) remains high.

The transformation of NO_x radicals into HNO_3, due to the occurrence of heterogeneous reactions at elevated water vapour amounts, affects stratospheric ozone chemistry. In the presence of a high NO_x concentration (as at low water vapour mixing ratios), ozone chemistry is dominated by NO_x radicals (see Sec. 3.1) and the ozone formation in cycle **C4** is determined by the rate of R19 (OH+CO). But if the NO_x concentration is low (as in the second phase of the mechanism), this ozone formation cycle is rate limited by R21 ($NO + HO_2$). For the standard case at 15 ppmv H_2O, both rates are shown in Fig. 4e. In the first phase before NO_x is transferred into HNO_3, cycle **C4** is limited by R19 (OH+CO) which peaks on 1 August 2013 with a maximum rate of $1.0 \cdot 10^5$ cm^{-3}s^{-1}. In the second phase at low NO_x concentrations, cycle **C4** is limited by R21 ($NO + HO_2$) which peaks on 3 August 2013 with a maximum rate of $1.5 \cdot 10^4$ cm^{-3}s^{-1}. Hence, due to the occurrence of the heterogeneous reaction R1 the net ozone formation decreases by at least $3.5 \cdot 10^4$ cm^{-3}s^{-1} from 1 August to 3 August.

Atmos. Chem. Phys. Discuss., https://doi.org/10.5194/acp-2018-1193
Manuscript under review for journal Atmos. Chem. Phys.
Discussion started: 12 December 2018

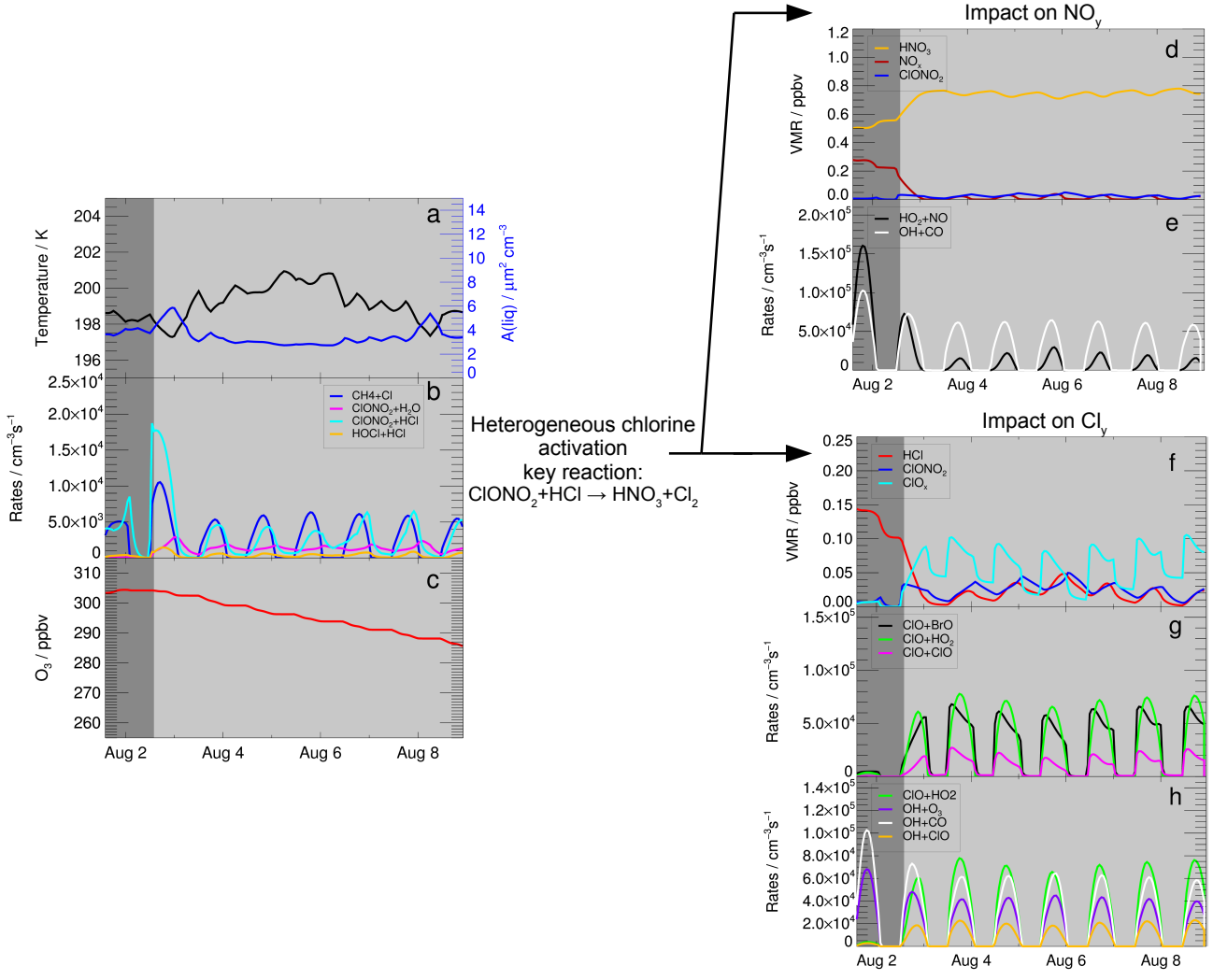

Figure 4. Reaction rates and mixing ratios important for the ozone loss mechanism in the standard simulation using 15 ppmv H_2O. The chlorine activation phase is shaded in dark grey, while the phase of ozone loss has an light grey background. Panel (a) shows the temperature of the trajectory and the liquid surface area density, the ozone mixing ratio is presented in panel (c). Heterogeneous reaction rates are shown in panel (b) as well as the rate of the gas phase reaction $CH_4 + Cl$. Panels (d), mixing ratio of HNO_3, NO_x and $ClONO_2$, and (e) are relevant to show the role of NO_y for the ozone loss process. Reaction R19 (OH+CO, panel e) limits ozone formation in cycle **C4** at high NO_x mixing ratios and R21 ($HO_2 + NO$ at lower NO_x concentrations. Panels (f)–(h) illustrate the role of chlorine for ozone loss by showing the mixing ratio of HCl, ClO_x and $ClONO_2$ (panel f), main reaction rates (R4 (ClO+ClO), R8 (ClO+BrO), R10 ($ClO + HO_2$)) for catalytic ozone loss cycles (panel g) and potential pathways for the OH-radical (R19 (OH+CO), R26 (OH+ClO), R12 ($OH+O_3$)) as possible reaction chains following R10 ($ClO+HO_2$) (panel h).

Atmos. Chem. Phys. Discuss., https://doi.org/10.5194/acp-2018-1193
Manuscript under review for journal Atmos. Chem. Phys.
Discussion started: 12 December 2018

Atmospheric Chemistry and Physics Discussions

3.2.2 Role of ClO_x

In the first phase of the mechanism, chlorine activation yields a transformation of inactive chlorine into active ClO_x. Net chlorine activation occurs when the rates of the heterogeneous reactions R1($ClONO_2 + HCl$), R2 ($ClONO_2 + H_2O$) and R3 (HCl+HOCl) exceed the gas phase HCl formation dominated by the reaction

$$Cl + CH_4 \rightarrow HCl + CH_3. \quad \text{(R24)}$$

Enhanced ClO_x concentrations induce catalytic ozone loss cycles at low temperatures, as the ClO-Dimer-cycle (**C1**) (Molina et al., 1987), the ClO-BrO-cycle (**C2**) (McElroy et al., 1986) and cycle **C3** (Solomon et al., 1986). Under conditions of low water vapour (stratospheric background) the rate limiting steps of these cycles are the reactions

$$ClO + ClO + M \rightarrow ClOOCl + M, \quad \text{(R4)}$$

$$ClO + BrO \rightarrow Br + Cl + O_2 \quad \text{(R8)}$$

$$\text{and} \quad ClO + HO_2 \rightarrow HOCl + O_2. \quad \text{(R10)}$$

The rates of reactions R4, R8 and R10 increase strongly in the second phase of the mechanism (light grey area in Fig. 4g) and thus catalytic ozone loss cycles can occur. Under the assumed conditions, ozone depletion is mainly driven by reaction pathways following both R8 and R10. The reaction rates peak on August 3 with a value of $7.8 \cdot 10^4\,cm^{-3}s^{-1}$ for R10 (ClO+HO_2), $6.8 \cdot 10^4\,cm^{-3}s^{-1}$ for R8 (ClO+BrO) and $2.7 \cdot 10^4\,cm^{-3}s^{-1}$ for R4 (ClO+ClO). In contrast the rate of ozone loss due to the reactions

$$ClO + O(^3P) \rightarrow Cl + O_2 \quad \text{(R25)}$$

$$Cl + O_3 \rightarrow ClO + O_2 \quad \text{(R7)}$$

$$\text{net: } O(^3P) + O_3 \rightarrow 2\,O_2$$

are not important here, as the peak values or R25 are only about $0.35 \cdot 10^4\,cm^{-3}s^{-1}$(not shown).

Additionally the sensitivity of various reaction rates to the water vapour mixing ratio was tested. In Figure 5, the mean reaction rates on 3 August are plotted against the water content assumed during the simulation. Panel (a) shows an acceleration of the ozone loss cycles **C2** (based on R8) and **C3** (based on R10) beginning from a water vapour mixing ratio of 11ppmv. In contrast, the rate determining reaction of **C1** (R4, ClO+ClO) increases at a higher water vapour mixing ratio.

At stratospheric background conditions with a low water vapour mixing ratio, the rate determining step of cycle **C3** is R10 (Solomon et al., 1986; Ward and Rowley, 2016). For the conditions with enhanced water vapour of 15 ppmv in the standard simulation, the rate of R12 (OH+O_3) is limiting this cycle (Fig. 4f). An investigation of possible reaction pathways of the OH-radical yields that reactions of OH with CO (R19) and ClO (R26) exhibit a rate similar to the reaction with ozone (R12, Fig. 5b).

$$OH + CO \rightarrow H + CO_2 \quad \text{(R19)}$$

$$OH + ClO \rightarrow HO_2 + Cl \quad \text{(R26)}$$

Atmos. Chem. Phys. Discuss., https://doi.org/10.5194/acp-2018-1193
Manuscript under review for journal Atmos. Chem. Phys.
Discussion started: 12 December 2018

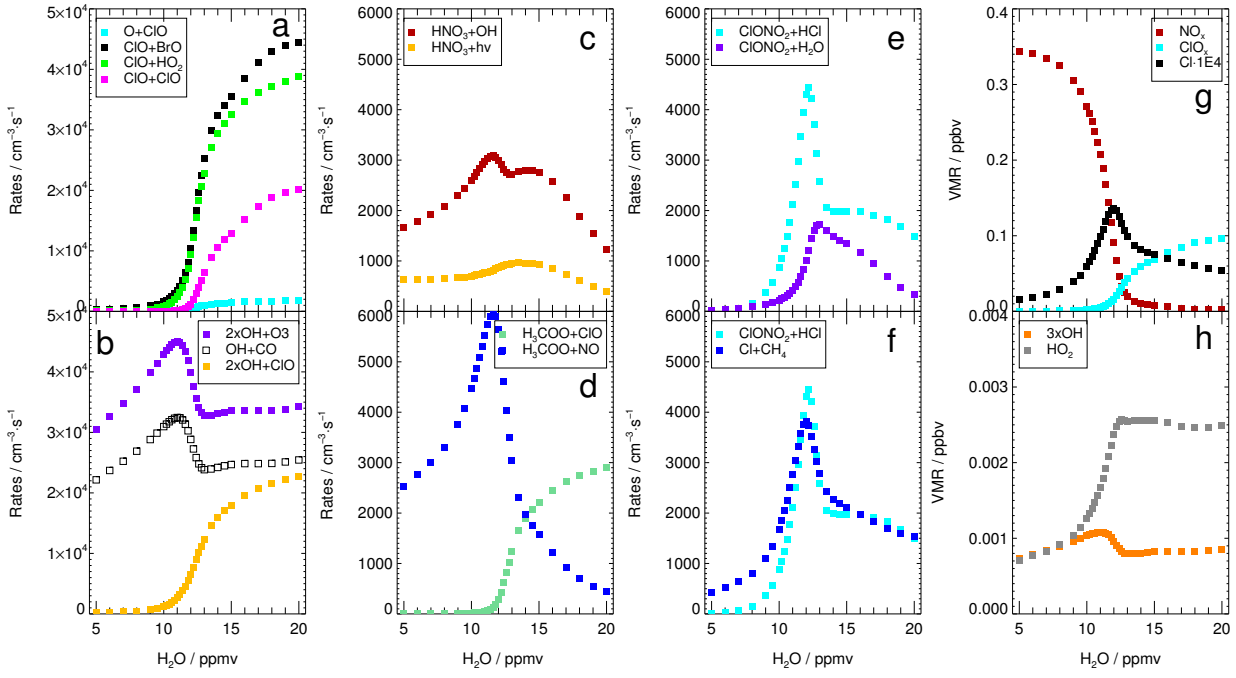

Figure 5. Average reaction rates and volume mixing ratios from the standard simulations on 3rd of August dependent on water vapour content. Panel (a) shows the reaction rates of R4 (ClO+ClO), R8 (ClO+BrO), R10 ($ClO + HO_2$) and R25 (ClO+O(3P)) resulting in ozone reduction, panel (b) possible reaction pathways for the OH radical (R19 (OH+CO), R26 (OH+ClO) and R12 ($OH+O_3$), panel (c) reactions yielding depletion of HNO_3 (R31 ($HNO_3 + OH$), R34 ($HNO_3 + h\nu$), panel (d) reactions of the H_3COO-radical R27 ($H_3COO + ClO$) and R29 ($H_3COO + NO$), panel (e) important heterogeneous reactions (R1 ($ClONO_2 + HCl$), R2 ($ClONO_2 + H_2O$)), and panel (f) the balance between R1 ($ClONO_2 + HCl$) and R24 ($CH_4 + Cl$). Panel (g) shows the mixing ratios of NO_x, ClO_x and 10·Cl and panel (h) the mixing ratios of OH and HO_2.

Based on these reactions, two further reaction chains affecting ozone can be deduced. In cycle **C5** the OH-radical reacts with CO yielding CO_2 and a hydrogen radical, from which HO_2 is formed. Subsequently HOCl can be formed via R10 ($ClO+HO_2$) and photolysed in reaction R11. Thus, the net reaction of this pathway is the oxidation of CO to CO_2 and the simultanous

destruction of ozone (**C5**).

$$OH + CO \rightarrow H + CO_2 \quad \text{(R19)}$$

$$H + O_2 + M \rightarrow HO_2 + M \quad \text{(R20)}$$

$$ClO + HO_2 \rightarrow HOCl + O_2 \quad \text{(R10)}$$

$$HOCl + h\nu \rightarrow Cl + OH \quad \text{(R11)}$$

$$Cl + O_3 \rightarrow ClO + O_2 \quad \text{(R7)}$$

$$\text{net: } CO + O_3 + h\nu \rightarrow CO_2 + O_2 \quad \textbf{(C5)}$$

Furthermore, when the OH-radical reacts with ClO, the products are HO_2 and Cl and thus another catalytic ozone loss cycle **C6** results.

$$OH + ClO \rightarrow HO_2 + Cl \quad \text{(R26)}$$

$$ClO + HO_2 \rightarrow HOCl + O_2 \quad \text{(R10)}$$

$$HOCl + h\nu \rightarrow Cl + OH \quad \text{(R11)}$$

$$2\text{ x } (Cl + O_3 \rightarrow ClO + O_2) \quad \text{(R7)}$$

$$\text{net: } 2O_3 \rightarrow 3O_2 \quad \textbf{(C6)}$$

In the cycles **C3** and **C6** two ozone molecules are destroyed, while one ozone molecule is destroyed in **C5**. To assess the effectiveness regarding ozone loss of **C3** and **C5** – **C6**, the rate of R19 (limiting **C5**) is compared with two times the rate of R12 (limiting **C3**) and R26 (limiting **C6**). This comparison shows that cycle **C3** is more relevant for ozone loss than **C5** and **C6** (Fig. 5b). Reaction R12 (**C3**) and R19 (**C5**) accelerate with increasing water vapour mixing ratio, due to an increasing formation of OH (Fig. 5h), and peak in the threshold range of ∼11 ppmv H_2O. When the threshold region is reached, the OH mixing ratio decreases due to a declining NO_x mixing ratio (Fig. 5g) and thus a lower rate of the reaction

$$HO_2 + NO \rightarrow OH + NO_2. \quad \text{(R21)}$$

The lower OH concentration results in a decrease of the reaction rates of R12 (OH+O_3) and R19 (OH+CO) shown in Fig. 5b, since R12 (OH+O_3) and R19 (OH+CO) are limited through the OH mixing ratio. The limiting step of cycle **C6** (R26) is negligible for low water amounts and starts to increase in the range of the threshold region due to the strong gain of both ClO_x and HO_2 (Fig. 5g-h). Accordingly the relevance of **C6** for catalytic ozone destruction increases for higher water vapour mixing ratios.

A requirement for the effectiveness of the ozone loss cycles **C1** – **C3** and **C5** – **C6** is a high mixing ratio of active chlorine (ClO_x). In Fig. 4b, the rate of the main HCl-formating reaction R24 (Cl+CH_4, dark blue) shows a formation of HCl, which has to be balanced (by HCl destroying reactions) to hold the HCl mixing ratio low and thus ClO_x values high. For conditions of the Antarctic polar night in the lower stratosphere this balance between gas phase HCl-formation and heterogeneous

Atmos. Chem. Phys. Discuss., https://doi.org/10.5194/acp-2018-1193
Manuscript under review for journal Atmos. Chem. Phys.
Discussion started: 12 December 2018

Atmospheric Chemistry and Physics Discussions

HCl-destruction can be described through HCl-null-cycles (Müller et al., 2018). In these HCl-null-cycles each HCl formed in reaction R24 is depleted through the heterogeneous reaction R3 (HCl+HOCl). For the formation of HOCl in reaction R10 (HO_2+ClO), the generation of HO_2 radicals through R27 is essential for Antarctic polar night conditions.

$$H_3COO + ClO \rightarrow HCHO + HO_2 + Cl \quad \text{(R27)}$$

For the conditions in the mid-latitudes during summer considered here, a higher NO_x mixing ratio prevails than under Antarctic ozone hole conditions due to a lower HNO_3 uptake into the condensed particles. As a consequence R1 ($ClONO_2 + HCl$) is mainly responsible for the HCl-loss and hence the pathway **C7** represents a more probable reaction chain to balance the HCl-formation.

$$Cl + CH_4 \rightarrow HCl + CH_3 \quad \text{(R24)}$$

$$CH_3 + O_2 \rightarrow H_3COO \quad \text{(R28)}$$

$$H_3COO + NO \rightarrow NO_2 + H_3CO \quad \text{(R29)}$$

$$H_3CO + O_2 \rightarrow HCHO + HO_2 \quad \text{(R30)}$$

$$NO_2 + h\nu \rightarrow NO + O(^3P) \quad \text{(R15)}$$

$$HO_2 + ClO \rightarrow HOCl + O_2 \quad \text{(R10)}$$

$$HOCl + h\nu \rightarrow OH + Cl \quad \text{(R11)}$$

$$OH + HNO_3 \rightarrow H_2O + NO_3 \quad \text{(R31)}$$

$$NO_3 + h\nu \rightarrow NO_2 + O(^3P) \quad \text{(R32)}$$

$$ClO + NO_2 + M \rightarrow ClONO_2 + M \quad \text{(R22)}$$

$$ClONO_2 + HCl \rightarrow HNO_3 + Cl_2 \quad \text{(R1)}$$

$$Cl_2 + h\nu \rightarrow 2Cl \quad \text{(R23)}$$

$$2 \times (O(^3P) + O_2 + M \rightarrow O_3 + M) \quad \text{(R33)}$$

$$2 \times (Cl + O_3 \rightarrow ClO + O_2) \quad \text{(R7)}$$

$$\text{net: } CH_4 + O_2 \rightarrow HCHO + H_2O \quad \textbf{(C7)}$$

Since the reactions R24, R29, R31 and R1 hold the lowest rates in **C7**, these reactions are essential for constituting **C7**. In R24 HCl is formed and afterwards instantly a methylperoxy radical (H_3COO) is formed (R28), which reacts with NO (R29). This reaction yields an H-radical, which is rapidly converted into an OH-radical by formation and photolysis of HOCl (R10 and R11). Through the reaction between the OH-radical and HNO_3 (R31) and the subsequent photolysis of NO_3 (R32), a NO_2-radical is released from HNO_3. The photolysis of HNO_3

$$HNO_3 + h\nu \rightarrow NO_2 + OH \quad \text{(R34)}$$

might be a further option to convert HNO_3 into active NO_x, but the rate of reaction OH+HNO_3 (R31) is more than 2.5 times larger than the rate of the HNO_3 photolysis (Fig. 5c). The NO_2-radical, which is generated in R32, reacts with ClO (R22)

forming $ClONO_2$, which heterogeneously reacts with HCl (R1). As a consequence the HCl, formed in reaction R24, is mainly destroyed in reaction R1 following pathway **C7**, which yields the oxidation of CH_4 as the net reaction.

In cycle **C7** the H_3COO-radical reacts with NO (R29). As an alternative the H_3COO-radical can also react with ClO (R27). In Fig. 5d the rates of R29 and R27 are compared with each other dependent on the water vapour mixing ratio assumed during the simulation. For the water vapour mixing ratio of the threshold region, reaction R29 dominates and **C7** mainly balances the HCl-formation and destruction. At higher water vapour mixing ratios (more than 15 ppmv), reaction R27 (H_3COO+ClO) becomes more important than R29 (H_3COO+NO, Fig. 5c), because of a lower NO_x and a higher ClO_x concentration. The lower NO_x mixing ratio is due to a stronger conversion of NO_x into HNO_3 as well as a higher HNO_3 uptake into the liquid particles at a higher water vapour mixing ratio. Hence for very high water vapour mixing ratios (here, greater than 15 ppmv), cycle **C8** mainly balances HCl formation.

$$Cl + CH_4 \rightarrow HCl + CH_3 \quad \text{(R24)}$$
$$CH_3 + O_2 \rightarrow H_3COO \quad \text{(R28)}$$
$$H_3COO + ClO \rightarrow HCHO + HO_2 + Cl \quad \text{(R27)}$$
$$HO_2 + ClO \rightarrow HOCl + O_2 \quad \text{(R10)}$$
$$HOCl + h\nu \rightarrow OH + Cl \quad \text{(R11)}$$
$$OH + HNO_3 \rightarrow H_2O + NO_3 \quad \text{(R31)}$$
$$NO_3 + h\nu \rightarrow NO_2 + O(^3P) \quad \text{(R32)}$$
$$ClO + NO_2 + M \rightarrow ClONO_2 + M \quad \text{(R22)}$$
$$ClONO_2 + HCl \rightarrow HNO_3 + Cl_2 \quad \text{(R1)}$$
$$Cl_2 + h\nu \rightarrow 2Cl \quad \text{(R23)}$$
$$O(^3P) + O_2 + M \rightarrow O_3 + M \quad \text{(R35)}$$
$$3 \times (Cl + O_3 \rightarrow ClO + O_2) \quad \text{(R7)}$$
$$\text{net: } CH_4 + 2O_3 \rightarrow HCHO + H_2O + 2O_2 \quad \textbf{(C8)}$$

The net reaction of **C8** is the oxidation of methane (CH_4) into formaldehyde (HCHO) with a simultaneous ozone destruction. Since the ozone destruction due to the catalytic ozone loss cycles **C2** and **C5** is much faster, the ozone destruction in **C8** is negligible compared to the ozone loss cycles discussed above.

However, in this example the heterogeneous HCl-destruction (R1) does not balance the HCl-formation (R24) (Fig. 4b) due to increasing temperatures (Fig. 4a). Higher temperatures decelerate the heterogeneous HCl-destruction and thus result in the slightly increasing HCl-mixing ratio from 4 August–7 August 2013 (Fig. 4f). Such temperature fluctuations (Fig. 4a) affect the balance between HCl formation and destruction less at higher water vapour mixing ratios, because the heterogeneous HCl-destruction rate (R1) increases for both low temperatures and high water vapour mixing ratios (see Sec. 4). Thus, regarding the balance between HCl formation and HCl destruction (and hence the balance between chlorine deactivation and chlorine

activation), a high water vapour mixing ratio can compensate a small range of temperature fluctuations. This balance can be described by the cycles **C7** and **C8** and maintains active chlorine levels, which is essential for the ozone loss cycles **C1–C3** and **C5–C6** to proceed.

4 Analysis of chlorine activation

In the previous section we showed that in the temperature range of 197–203 K there is a threshold for water vapour, which has to be exceeded to yield substantial ozone destruction. Here we investigate the sensitivity of this threshold on sulphate content, temperature, Cl_y and NO_y mixing ratio.

4.1 Sensitivity of the water vapour threshold

Modifying temperature, sulphate amount or the mixing ratios of Cl_y or NO_y yields a shift of the water vapour threshold. Figure 6 shows the ozone values reached at the end of the 7-day simulation (final ozone) for a variety of sensitivity cases assuming the standard trajectory of the SEAC^{4}RS case (left) and the MACPEX trajectory (right).

The water vapour dependent final ozone values for the standard case are plotted as blue squares (Fig. 6, left). Raising the trajectory temperature by 1 K over the standard case leads to a higher water vapour threshold of 13.5–14.0 ppmv (open red squares), while increasing the sulphate content by a factor of 3 results in a lower threshold region of 9.0–9.5 ppmv (yellow diamonds). An even larger enhancement of the sulphate content (10× H_2SO_4, magenta diamonds) lowers the water vapour threshold further to a value near 7 ppmv. Reducing the NO_y mixing ratio to 80% of the standard case yields a shift of the threshold to a lower water vapour mixing ratio (green filled triangles), while an equivalent reduction in the Cl_y mixing ratio shifts the threshold region to higher water vapour mixing ratios (black circles). A reduction in Cl_y also results in higher ozone mixing ratios at the end of the simulation.

While the preceding analysis was based on a single SEAC^{4}RS trajectory, similar conclusions are reached when the analysis is conducted using a trajectory from the MACPEX campaign. Results of the analysis using the MACPEX initialization and backward trajectory (Fig. 1, black) are shown in the right panel of Fig. 6. A critical water vapour range of 12–13 ppmv is required to produce a reduction of the final ozone value. In the MACPEX case, the final ozone is mostly for all simulations higher than the initial ozone. This is due to the lower Cl_y-mixing ratio (∼55 pptv) assumed in the MACPEX case, which yields lower rates for catalytic ozone loss after chlorine activation occurred. For the MACPEX case, changes in sulphate (Fig. 6, left, yellow diamonds), Cl_y (black circles) or NO_y (green triangles) mixing ratios affect the catalytic ozone destruction water vapour threshold similarly to that observed for the SEAC^{4}RS trajectory. This yields the conclusion that in the considered temperature range (∼197–203 K), an ozone reduction occurs after exceeding a water vapour threshold and that this threshold varies with Cl_y, NO_y, sulphate content and temperature.

Atmos. Chem. Phys. Discuss., https://doi.org/10.5194/acp-2018-1193
Manuscript under review for journal Atmos. Chem. Phys.
Discussion started: 12 December 2018

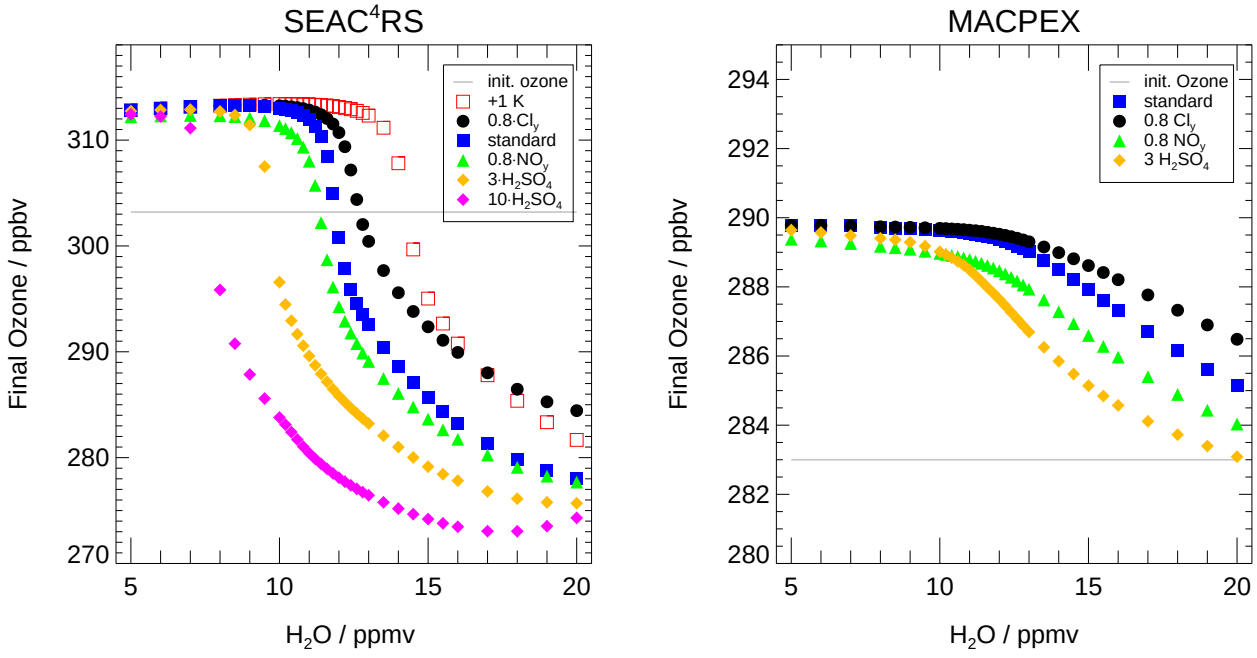

Figure 6. Impact of the water vapour content on the ozone mixing ratio (final ozone) reached at the end of the 7-day simulation along the standard trajectory (SEAC^{4}RS, left) and the MACPEX trajectory (right). The standard case is shown in blue and the initial ozone amount is marked by the grey line. An impact on the final ozone mixing ratios is observable after exceeding a critical threshold in water vapour. This threshold changes with a shift in trajectory temperature (+1K, red), the Cl_y mixing ratio to 0.8 Cl_y (black), the NO_y mixing ratio (0.8 NO_y, green) and the sulphate content (3× standard H_2SO_4, yellow and 10× standard H_2SO_4, magenta).

4.2 Explanation of the water vapour threshold

The sensitivity of the water vapour threshold to Cl_y, NO_y, sulphate loading and temperature is investigated, focussing on the balance between heterogeneous chlorine activation mainly due to R1 ($ClONO_2 + HCl$) and gas phase chlorine deactivation mainly due to R24 ($Cl + CH_4$). Net chlorine activation takes place when the chlorine activation rate exceeds the chlorine deactivation rate. Reaction R1 is the key reaction in the chlorine activation process. Therefore, in the following, first the dependency of R1 on the water vapour content is analysed in detail. Second, the balance between chlorine activation and deactivation is investigated, also considering the impact of Cl_y, NO_y sulphate and temperature on the threshold.

Atmos. Chem. Phys. Discuss., https://doi.org/10.5194/acp-2018-1193
Manuscript under review for journal Atmos. Chem. Phys.
Discussion started: 12 December 2018

Atmospheric Chemistry and Physics Discussions

In general the rate of R1 ($ClONO_2 + HCl$) v_{R1} is determined through:

$$v_{R1} = k_{R1} \cdot c_{ClONO_2} \cdot c_{HCl} \quad (1)$$

The concentrations of $ClONO_2$ c_{ClONO_2} and HCl c_{HCl} are associated with the gas phase mixing ratio and the rate constant k_{R1}, as a measure of the reactivity of the heterogeneous reaction, depends in this case on the γ-value γ_{R1}, the surface area of the liquid particle A_{liq}, the temperature T and c_{HCl} (Eq. 2) (Shi et al., 2001).

$$k_{R1} \propto \frac{\gamma_{R1} \cdot A_{liq} \cdot \sqrt{T}}{1 + c_{HCl}} \quad (2)$$

The γ-value describes the uptake of $ClONO_2$ into liquid particles due to the decomposition of $ClONO_2$ during reaction R1 and is thus a measure of the probability of the occurrence of this heterogeneous reaction (Shi et al., 2001). From Eq. 2 it is obvious that a large surface area A_{liq} and a high γ-value γ_{R1} increase k_{R1} and thus the heterogeneous reaction rate v_{R1}.

In Figure 7, the impact of the water vapour content on γ_{R1}, A_{liq}, k_{R1} and the reaction rate v_{R1} is plotted. To avoid the influence of R1 itself on these parameters as much as possible, these parameters are selected for 1 August 2013 at 13:00 UTC. This point in time corresponds to the values after the first chemistry time step during the chemical simulation. The standard case is illustrated in blue squares (Fig.7) and exhibits a strongly increasing gamma value especially for water vapour mixing ratios between 9 and 14 ppmv as well as an almost constant liquid surface area A_{liq} in the same water vapour range. The slight increase in A_{liq} is caused by HNO_3 formation in R1 and the subsequent uptake of HNO_3 into the condensed particles, especially for high water values. Due to an increasing γ-value with increasing water vapour, the rate constant k_{R1} increases (Shi et al., 2001) and thus induces a larger reaction rate v_{R1} with an increasing water vapour mixing ratio.

At low water vapour mixing ratios, not only the rate of R1 ($ClONO_2 + HCl$) but also of R24 ($CH_4 + Cl$) increases with an increasing water content (Fig. 5f). An increasing heterogeneous reaction rate (R1) results in both a lower NO_x mixing ratio and more HCl converted into ClO_x. A higher ClO_x concentration yields a higher Cl mixing ratio and thus an increase in the rate of R24 ($CH_4 + Cl$). Since both the rates of R1 and R24 increase, no significant net chlorine activation occurs. In the water vapour threshold region, the Cl-mixing ratio peaks (Fig. 5g), because less ClO is converted into Cl through R17 (ClO+NO) due to the decreasing NO_x mixing ratio. The lower Cl mixing ratio reduces the HCl formation in R24 ($CH_4 + Cl$). Hence, the increasing heterogeneous reactivity k_{R1} impedes R24 by reducing the NO_x mixing ratio. In the same way, an increase in k_{R1} yields a higher rate of R1. As a consequence the rate of R1 exceeds the rate of R24 and a net chlorine activation takes place, leading to a reduction of HCl. The decline in both HCl and NO_x yields smaller rates of R1 and R24 at high water amounts and thus the peak of R1 and R24 occurs in the water vapour threshold region (Fig. 5f). Hence, the increasing heterogeneous reactivity (k_{R1}) of R1 promotes chlorine activation (due to an increasing rate of R1) and impedes chlorine deactivation (due to a reduction of R24). This yields heterogeneous chlorine activation to exceed gas phase HCl-formation in the water vapour threshold region. The increase in k_{R1} yields a net chlorine activation in the water vapour threshold region by destabilizing the balance between chlorine activation and deactivation.

For an enhanced sulphate content (Fig. 7, yellow diamonds), the particle surface area density (illustrated by A_{liq}) is larger, leading to both a stronger increase of the heterogeneous reactivity (k_{R1}) and a higher heterogeneous reaction rate than in the

Atmos. Chem. Phys. Discuss., https://doi.org/10.5194/acp-2018-1193
Manuscript under review for journal Atmos. Chem. Phys.
Discussion started: 12 December 2018

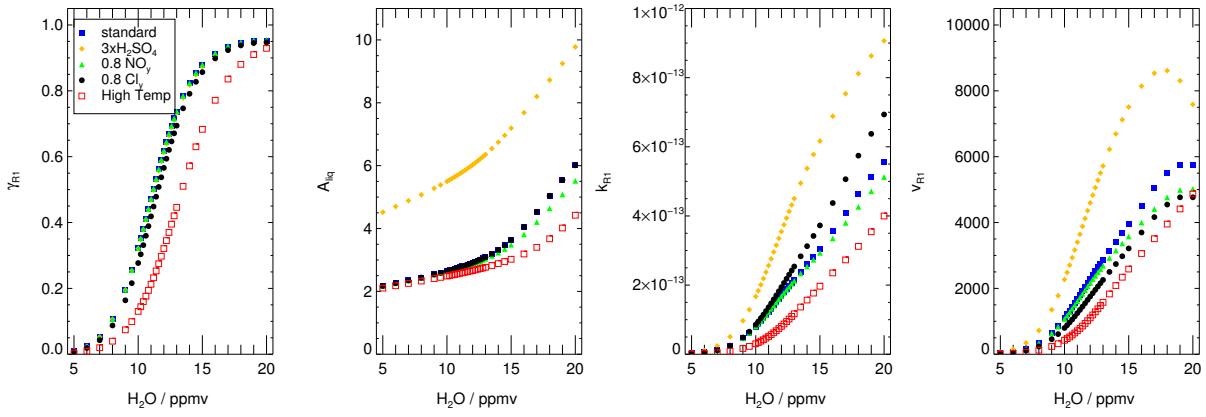

Figure 7. Dependence on water vapour of the rate of the the main heterogeneous chlorine activation reaction R1, the rate coefficient (k_{R1}), the γ-value γ_{R1} and the liquid surface area density A_{liq}. Presented parameters correspond to the values after the first chemistry time step of the box-model simulation. Additionally the impact of an enhanced sulphate content (0.8 ppbv H_2SO_4, yellow), reduced NO_y (0.8 NO_y, green), reduced Cl_y (0.8 Cl_y, black) and enhanced temperatures (red) is shown. The standard case is shown as blue squares.

standard case. Due to this higher heterogeneous reactivity (k_{R1}), the chlorine activation rate exceeds the chlorine deactivation at a lower water vapour mixing ratio and the net chlorine activation is reached at a lower water vapour threshold. A shift to higher temperatures (Fig. 7, red) yields almost no change in the surface area density (A_{liq}) but a reduced γ-value and thus a lower heterogeneous reactivity (k_{R1}). The reduced reactivity causes the net chlorine activation to occur at a higher water vapour threshold. In contrast, the shift of the threshold for simulations with only 80% of standard NO_y (0.8 NO_y, Fig. 7 green) or Cl_y (0.8 Cl_y, Fig. 7 black) can not be explained only by an increase in k_{R1}. In these cases, further effects on the balance between chlorine activation and chlorine deactivation have to be taken into account. The water vapour threshold in the 0.8 NO_y simulation (green triangles) is shifted to lower water vapour values due to a smaller Cl/ClO-ratio for lower NO_x concentrations. This yields a reduced HCl formation through R24 ($CH_4 + Cl$) than in the standard case and thus impedes chlorine deactivation.

Atmos. Chem. Phys. Discuss., https://doi.org/10.5194/acp-2018-1193
Manuscript under review for journal Atmos. Chem. Phys.
Discussion started: 12 December 2018

The reduced chlorine deactivation affects the balance between chlorine activation and deactivation in a way that the water vapour threshold region in the 0.8 NO_y case is lower than in the standard case. In the 0.8 Cl_y case (Fig. 7, black), the HCl and $ClONO_2$ mixing ratios are reduced. This leads to a lower chlorine activation rate v_{R1} than in the standard case, despite of the slight higher heterogeneous reactivity (k_{R1}), which is due to the inverse dependence of k_{R1} on the HCl concentration (Eq. 2). The lower dependence of reaction R24 (Cl+CH_4) than of R1 ($HCl + ClONO_2$) on the Cl_y mixing ratio would push chlorine deactivation (R24) in the balance between chlorine activation and deactivation and hence shift the water vapour threshold to higher water vapour mixing ratios. Additionally caused by the lower rate of R1 ($ClONO_2 + HCl$) for reduced Cl_y, the NO_x mixing ratio decreases more slowly. This enhances the rate of R24 compared with the standard case as well, because more NO_x yields a higher Cl/ClO-ratio.

In summary, the threshold is determined by the balance between chlorine activation and deactivation and is thus in a certain temperature range especially sensitive to the water dependence of the heterogeneous reactivity (k_{R1}) mainly described through the γ-value γ_{R1} and the particle surface A_{liq}. These parameters are dependent on the present temperature and sulphate content. However, further parameters shifting this balance, such as the NO_y and Cl_y mixing ratio, have an impact on the water vapour threshold as well.

4.3 Temperature dependence

The water vapour threshold, which has to be exceeded for chlorine activation and stratospheric ozone loss to occur, is mainly dependent on the temperature. To illustrate the impact of both temperature and water vapour mixing ratio on stratospheric ozone, the relative ozone change occurring after a 7-day simulation, in which a constant temperature and water vapour concentration and the Cl_y and NO_y of the standard case is assumed, is shown in Fig. 8. In the left panel, ozone change as a function of temperature and water vapour is plotted for non-enhanced sulphate amounts. In the right panel, the relative ozone change is shown for 10× standard sulphate to estimate a potential impact of sulphate geoengineering on stratospheric ozone. Since mixing of neighbouring air parcels is neglected in the box-model study, the relative ozone change calculated corresponds to the largest possible ozone change for the conditions assumed. A mixing of air is expected to reduce the water vapour mixing ratio during the time period of the 7-day trajectory and hence could stop ozone depletion before the end of the trajectory is reached. In addition to the relative ozone change, the threshold for chlorine activation is shown as a white line in both panels. When temperature is held constant, this threshold corresponds to the water vapour threshold discussed above. Chlorine activation occurs at higher water mixing ratios and lower temperatures relative to the white line plotted. Here, chlorine is defined to be activated, if the ClO_x/Cl_y ratio exceeds 10%.

For climatological non-enhanced sulphate amounts (Fig. 8, left), the temperature has to fall below 203 K for chlorine activation to occur, even for high water vapour mixing ratios of 20 ppmv. For the simultaneous presence of high water vapour and low temperatures an ozone loss of 9% (max. 27 ppbv O_3) was found. This maximal ozone loss occurs for a range of low temperatures (195–200 K) and enhanced water vapour mixing ratios (10–20 ppmv), because of a similar time until chlorine activation occurs. If the temperatures are higher and water vapour mixing ratios lower than the chlorine activation line, the ozone mixing ratio increases around 3.5% ($\sim$ 10 ppbv O_3). At enhanced sulphate conditions (Fig. 8, right) an ozone loss of

Atmos. Chem. Phys. Discuss., https://doi.org/10.5194/acp-2018-1193
Manuscript under review for journal Atmos. Chem. Phys.
Discussion started: 12 December 2018

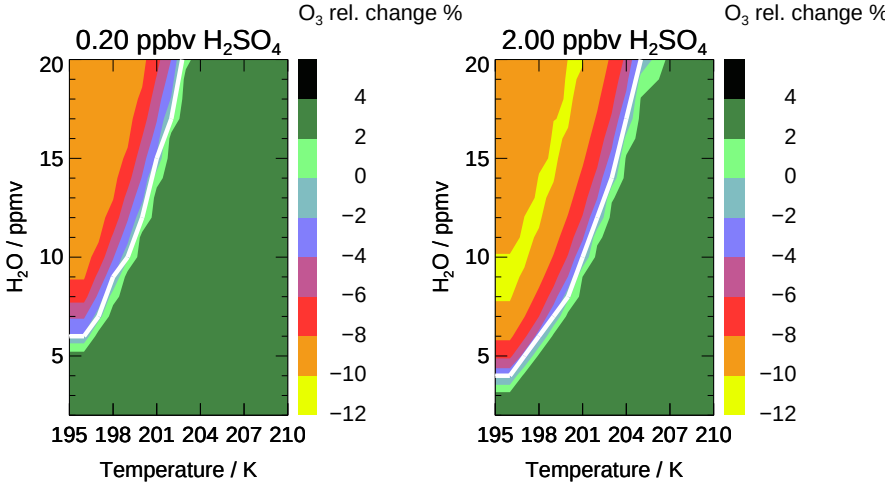

Figure 8. Relative ozone change during the 7-day simulation along the standard trajectory dependent on temperature and H_2O ratio for climatological non enhanced (left panel) and enhanced (right panel) sulphate conditions. The white line corresponds to the water and temperature dependent chlorine activation threshold.

max. 10% (30 ppmv O_3) occurs for low temperatures and high water vapour mixing ratios. For a water vapour mixing ratio of 20 ppmv the temperature has to fall below 205 K for ozone loss to occur. If the temperatures are very low (195–200 K) and the water vapour is high (10–20 ppmv) ozone loss is slightly reduced. This turnaround occurs, because at a high sulphate loading in combination with high water and low temperatures more HCl is taken up by condensed particles. This leads to less Cl_y in the gas phase and thus lower rates of catalytic ozone loss.

In summary, the combination of low temperatures, enhanced sulphate concentrations and high water vapour mixing ratios promotes an ozone decrease of up to ∼10% (max. −30 ppbv O_3) for high water vapour mixing ratios, low temperatures and enhanced sulphate conditions. In comparison to the study of Anderson et al. (2012), the temperatures have to fall below 203 K (here) instead of 205 K (in Anderson et al. (2012)) for non enhanced sulphate conditions and below 205 K instead of 208 K (in Anderson et al. (2012)) for enhanced sulphate conditions and a water vapour mixing ratio of 20 ppmv for chlorine activation and thus ozone loss to occur. Hence, Anderson et al. (2012) found ozone loss in mid-latitudes at high water vapour mixing ratios for temperatures 2 to 3 K higher than in our simulations.

Atmos. Chem. Phys. Discuss., https://doi.org/10.5194/acp-2018-1193
Manuscript under review for journal Atmos. Chem. Phys.
Discussion started: 12 December 2018

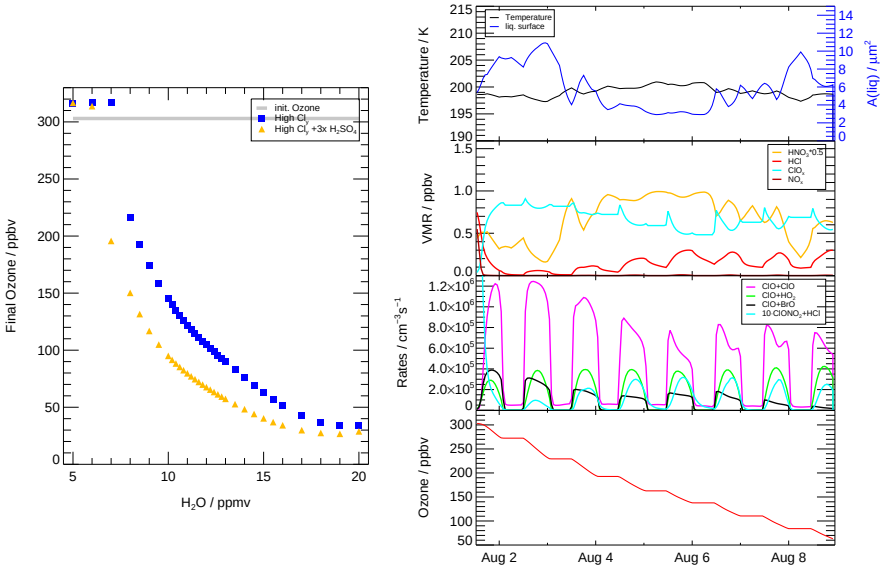

Figure 9. Behaviour under "Case of high Cl_y" conditions assuming high values for Cl_y and NO_y (see Tab. 1). Left panel shows the dependence of ozone values reached at the end of the 7-day simulation on water vapour for reference (blue) and 3×enhanced sulphate contents (yellow); the grey line corresponds to the initial ozone value. Right panel presents the volume mixing ratio of ozone, temperature, liquid surface density, mixing ratio of HNO_3 (scaled by 0.5), HCl, ClO_x and NO_x and reaction rates of reactions essential for chlorine activation and catalytic ozone loss cycles (R1 and R8 (ClO+BrO), R4 (ClO+ClO) and R10 ($ClO + HO_2$)).

5 Case studies

Case studies were conducted to illustrate the sensitivities described above on ozone loss and to estimate the impact of realistic conditions and an upper boundary on the ozone loss process. As a kind of worst case study (upper boundary), the "Case of high Cl_y" was simulated using Cl_y and NO_y mixing ratios based on the study of Anderson et al. (2012), which uses Cl_y and NO_y much larger than inferred from tracer-tracer correlations (Table 1). In the "case based on observations", standard conditions and the measured water vapour mixing ratio of 10.6 ppmv were assumed using both the low sulphate content of the standard case and a slightly enhanced sulphate content, which represents the possible impact of volcanic eruptions or geoengineering conditions. In the "reduced Br_y case", standard conditions with a 50% reduced Br_y mixing ratio were assumed to test uncertainties in current observations of stratospheric bromine burden. Additionally the previously noted standard 7-day trajectory was extended to a 19-day trajectory.

Atmos. Chem. Phys. Discuss., https://doi.org/10.5194/acp-2018-1193
Manuscript under review for journal Atmos. Chem. Phys.
Discussion started: 12 December 2018

5.1 Case of high Cl_y

Under conditions of substantially higher initial Cl_y and NO_y mixing ratios (see Tab. 1) than in the standard case used in Anderson et al. (2012), a larger ozone loss up to 265 ppbv during the 7-day simulation is simulated (Fig. 9). Since these high Cl_y conditions have been criticised in other studies (e.g. Schwartz et al., 2013; Homeyer et al., 2014) as being unrealistically high, they are assumed here as a worst case scenario. Under high chlorine conditions, and for a high water vapour content (more than ≈18 ppmv), an almost complete ozone destruction with an end ozone value of less than 50 ppbv is simulated (Fig. 9, left), which corresponds to parcel ozone loss of 85%. During the 3.5-day simulation in the study of Anderson et al. (2012), an ozone loss of 20% with respect to initial ozone occurs for 18 ppmv H_2O. This difference in relative ozone loss for similar conditions here and in the study of Anderson et al. (2012) is caused by a longer assumed ozone destruction period in our simulation. Assuming the measured water vapour content of 10.6 ppmv for high chlorine conditions would lead to an ozone depletion of 57% during the 7-day simulation. In comparison, in the standard case an ozone loss of 8% is reached when a high water vapour mixing ratio of 20 ppmv is assumed. However, even for the standard trajectory and a high chlorine content, a water vapour amount of 8 ppmv has to be exceeded to yield any ozone reduction. This threshold shifts from 8 ppmv to 7 ppmv for the case where stratospheric sulphate is tripled (Fig. 9, left, yellow triangles).

Comparing the standard case and the high Cl_y case using 15 ppmv water vapour conditions, in the high Cl_y case more inactive chlorine is converted into active ClO_x on the first day of the simulation (Fig. 9, right). This higher ClO_x mixing ratio results in faster catalytic ozone loss cycles with peak values of $3.9{\cdot}10^5 cm^{-3}s^{-1}$ for R10 (ClO+HO_2), $2.0{\cdot}10^5 cm^{-3}s^{-1}$ for R8 (ClO+BrO) and $10.9{\cdot}10^5 cm^{-3}s^{-1}$ for R4 (ClO+ClO) on 3 Aug 2013. Since the Cl_y-mixing ratio is much higher than in the standard case, the catalytic ozone loss cycles are dominated by the ClO-Dimer cycle and result in a much larger ozone loss than in the standard case assuming realistic Cl_y and NO_y mixing ratios.

5.2 Case based on observations

The simulation of the case based on observations during the SEAC^{4}RS aircraft campaign corresponds to the most realistic case for today's climate. It is identical to that of the standard case but assumes a fixed water vapour mixing ratio of 10.6 ppmv observed on 8 August 2013. Under these conditions, neither heterogeneous chlorine activation due to R1 ($ClONO_2 + HCl$) nor catalytic ozone loss cycles (e.g. based on ClO+BrO) can be observed in the simulation (Fig. 10, left). Instead, ozone is formed due to cycle **C4**. In comparison, the same simulation with 0.6 ppbv gas phase equivalent H_2SO_4 instead of 0.2 ppbv was conducted (Fig. 10, right). The enhanced sulphate content yields a larger liquid surface area density and thus an increased heterogeneous reactivity. Hence, reaction R1 occurs in the $3{\times}H_2SO_4$ simulation significantly, leading to a slightly increasing ClO_x mixing ratio and a decrease of the NO_x mixing ratio. Both a reduced ozone formation in **C4** (which is at decreased NO_x concentrations limited by R21) and ozone loss cycles (e.g. based on the reaction ClO+BrO or ClO+HO_2) can be observed, resulting in a reduction of ozone.

Using initial conditions, the trajectory corresponding to the SEAC^{4}RS observations shows ozone loss with sulphate enhanced by a factor of 3. However, we note that this was an unusually cold trajectory. A more common case with higher mean tem-

Atmos. Chem. Phys. Discuss., https://doi.org/10.5194/acp-2018-1193
Manuscript under review for journal Atmos. Chem. Phys.
Discussion started: 12 December 2018

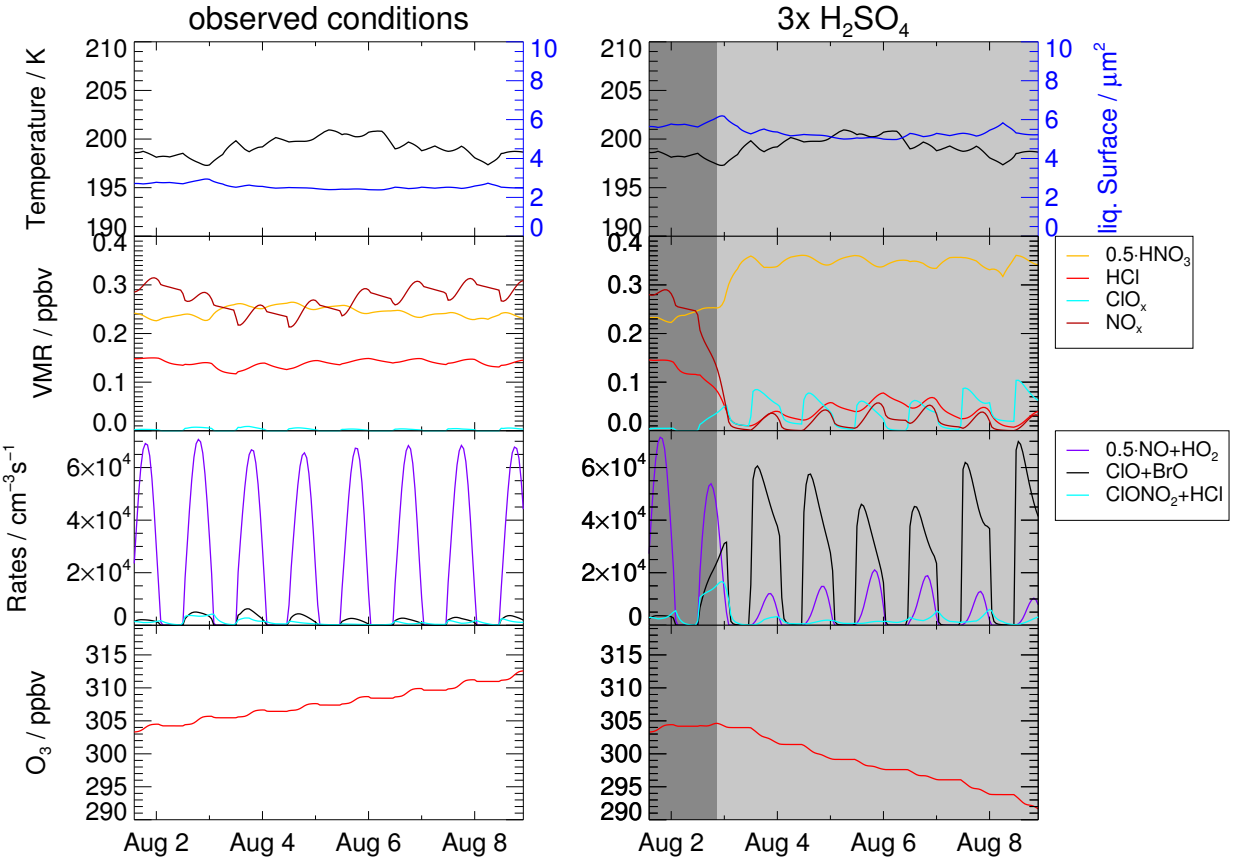

Figure 10. Left panels present the temperature, liquid surface area density, ozone mixing ratio, reaction rates of R1 ($ClONO_2 + HCl$, cyan), R8 (ClO+BrO, black) (as an example for ozone loss cycles), R21 ($NO + HO_2$, violet) which limits ozone formation at low NO_x concentrations as well as volume mixing ratios of HCl (red), ClO_x (light blue), NO_x (black) and HNO_3 (scaled with 0.5) for conditions of the measurement with 10.6 ppmv H_2O and 0.20 ppbv H_2SO_4. The panels on the right show the same quantities, but for enhanced sulphate conditions (0.60 ppbv H_2SO_4).

peratures would require a higher sulphate content to enhance the heterogeneous reactivity enough for chlorine activation to occur.

5.3 Reduced Br_y Case

The mixing ratio of inorganic bromine (Br_y) has a high uncertainty in the lowermost stratosphere due to the influence of very short lived bromine containing substances. For example, during the CONTRAST field campaign (Jan-Feb 2014, western Pacific region), Koenig et al. (2017) observed a Br_y mixing ratio in the lower stratosphere of 5.6–7.3 ppt and the contribution of Br_y, which crosses the tropopause, was estimated to be 2.1±2.1 ppt (Wales et al., 2018). Navarro et al. (2017) found somewhat

Atmos. Chem. Phys. Discuss., https://doi.org/10.5194/acp-2018-1193
Manuscript under review for journal Atmos. Chem. Phys.
Discussion started: 12 December 2018

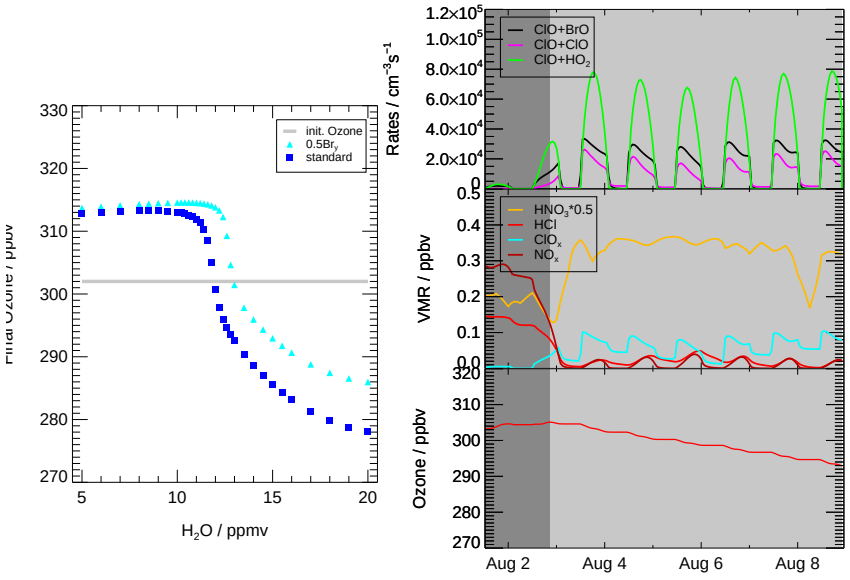

Figure 11. Impact of a Br_y reduction on the water vapour threshold and the ozone loss process. Left panel shows the dependence of ozone values reached at the end of the 7-day simulation on water vapour for the standard case (blue) and a simulation assuming the half of Br_y (light blue); the grey line corresponds to the initial ozone value. Right panel presents the volume mixing ratio of ozone, the mixing ratio of HNO_3 (scaled by 0.5), HCl, ClO_x and NO_x and reaction rates of reactions essential for chlorine activation and catalytic ozone loss cycles (R1 ($ClONO_2 + HCl$) and R8 (ClO+BrO), R4 (ClO+ClO) and R10 ($ClO + HO_2$)).

different bromine partitioning depending on the ozone, NO_2 and Cl_y concentrations, using very short lived bromine species observations in the eastern and western Pacific ocean from the ATTREX campaign. Because our Bry values are not based on measurements for this specific case modeled, we tested the sensitivity to a value that is half of our standard case. The impact of this Br_y reduction is illustrated in Fig. 11 assuming a water vapour mixing ratio of 15 ppmv.

Comparing the end ozone value for the 0.5 Br_y simulations (Fig. 11, left, light blue triangles) with those of the standard case (blue squares), a higher water vapour threshold and a reduced ozone loss at high water vapour mixing ratios is simulated. The reduction of Br_y yields a slightly longer time period of chlorine activation. At high HCl and low $ClONO_2$ mixing ratios at the start of the simulation, the formation of $ClONO_2$ in R22 (ClO+NO_2) is essential for maintaining the chlorine activation reaction R1 ($ClONO_2 + HCl$). Hence, the chlorine activation is dependent on the formation of $ClONO_2$ and thus on the NO_2/NO-ratio (von Hobe et al., 2011). A higher NO_2/NO-ratio yields a higher rate of R22 and enhances the rate of R1. A reduced Br_y-mixing ratio leads to a smaller NO_2/NO-ratio due to R18 (BrO+NO) and thus to a lower chlorine activation rate (von Hobe et al., 2011). A reduction of the chlorine activation rate (R1) would change the balance between chlorine activation and chlorine deactivation, which determines the water vapour threshold region. Thus, this reduction would lead to the shift of the water vapour threshold, which is illustrated in Fig. 11 (left panel). With less Br_y the catalytic ozone destruction in the ClO-BrO-cycle

Atmos. Chem. Phys. Discuss., https://doi.org/10.5194/acp-2018-1193
Manuscript under review for journal Atmos. Chem. Phys.
Discussion started: 12 December 2018

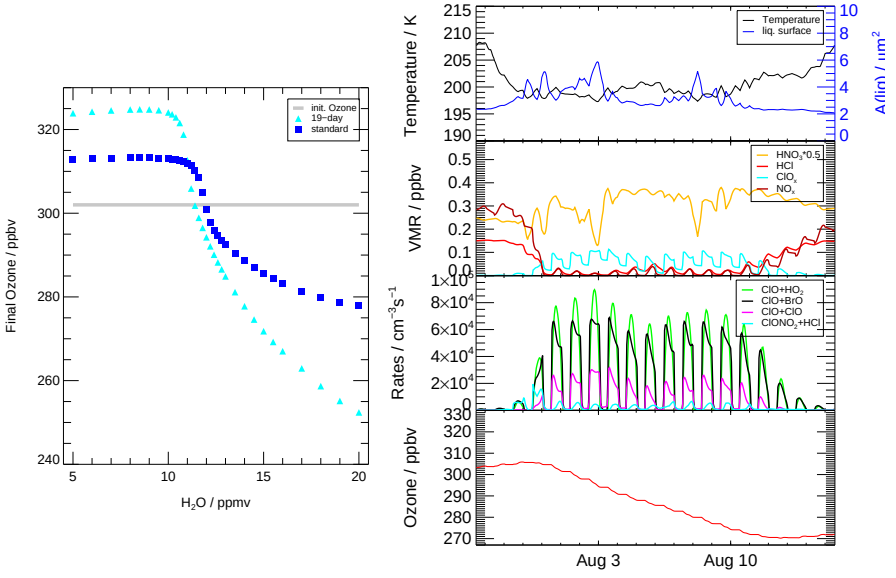

Figure 12. Impact of the simulated time period on ozone loss. Left panel shows the dependence of ozone values reached at the end of the simulation on water vapour for the standard case (7-day, blue) and the 19-day simulation (cyan); the grey line corresponds to the initial ozone value. Right panel presents temperature, liquid surface area, the mixing ratio of ozone, HNO_3 (scaled by 0.5), HCl, ClO_x and NO_x and reaction rates of reactions essential for chlorine activation and catalytic ozone loss cycles (R1 ($ClONO_2 + HCl$) and R8 (ClO+BrO), R4 (ClO+ClO) and R10 ($ClO + HO_2$)) for the 19-day simulation.

(**C2**) is reduced (Fig. 11, right panel), while the rates of R4 (ClO+ClO) and R10 (ClO+HO_2) are similar to those of the standard case (Fig. 4,e). This results in the reduced ozone destruction in the 0.5 Br_y case.

5.4 19-day simulation

Since the occurrence of the ozone loss process analysed in this study is strongly dependent on a variety of parameters, the time period over which the ozone loss might occur is very uncertain. The impact of this time period on ozone loss was tested by extending the 7-day trajectory used in the sections above to span the entire period with temperatures low enough to maintain chlorine activation. The temperature development of this trajectory is shown in Fig. 12. On 27 July 2013, the 19-day simulation starts at a temperature of 208 K (Fig. 12, right), decreasing until 29 July 2013 to lower than 200 K. The temperatures remain lower than 201 K until 11 August and increase to over 205 K on 14 August 2013.

Assuming a water vapour mixing ratio of 15 ppmv, chlorine activation occurs on 30 July 2013, after the temperatures fall below 200 K (Fig. 12, right). The mixing ratio of NO_x remains low and ClO_x remains high until 11 August, when the heterogeneous reaction rate of R1 ($ClONO_2 + HCl$) decreases due to higher temperatures. For this reason chlorine activation cannot anymore be maintained by cycle **C7**. Thus, the time span holding a ClO_x mixing ratio high enough for the occurrence of catalytic ozone

Atmos. Chem. Phys. Discuss., https://doi.org/10.5194/acp-2018-1193
Manuscript under review for journal Atmos. Chem. Phys.
Discussion started: 12 December 2018

loss cycles (**C1**–**C3**, **C5**–**C6**) comprises 14 days and ozone destruction stops on 12 August.

Because of the extended time period, the final ozone values using the enhanced water vapour mixing ratios for 19-days (cyan triangles Fig. 12, left panel) are much lower than those of the standard 7-day simulation (blue squares). Additionally, more ozone is formed when using low water vapour concentrations. Comparing the water vapour threshold of the 7-day trajectory (∼11.0–11.6 ppmv) and the 19-day simulation (∼10.6 ppmv), a shift to lower water vapour mixing ratios occurs in the 19-day trajectory. This shift is likely due to an extended time period with a temperature well below 200 K, which allows a chlorine activation to occur even for slightly lower water vapour amounts. Simulations along a trajectory starting on the same day as the 7-day trajectory, but finishing on 15 August, yield the same water vapour threshold as the 7-day simulation (not shown), indicating that the shift in the threshold shown in Fig. 12 is associated with the very cold conditions at the start of the 19-day simulation. Hence, the length of the chosen trajectory has no impact on the water vapour threshold, but does effect the final ozone.

6 Discussion

Many uncertainties affect the assessment of the extent of ozone loss that occurs in the lowermost stratosphere at mid-latitudes under elevated water vapour conditions. The number and depth of convective overshooting events as well as the area and duration affected by enhanced water vapour mixing ratios is a subject of recent research (e.g. Homeyer et al., 2014; Smith et al., 2017). The mixing ratio of important trace gases (O_3, Cl_y, Br_y, NO_y) in overshooting plumes and the possibility that water vapour mixing ratios high enough for chlorine activation meet temperatures low enough is a matter of debate (e.g. Schwartz et al., 2013; Homeyer et al., 2014). In this study, we examined the sensitivity to different water vapour mixing ratios, temperature, H_2SO_4 content, Cl_y, NO_y, Br_y and trajectory duration.

The ozone loss mechanism investigated here requires the occurrence of the heterogeneous reaction R1, which leads to enhanced ClO_x and reduced NO_x mixing ratios and thus maintains effective catalytic ozone loss cycles. Enhanced ClO and reduced NO concentrations were observed by Keim et al. (1996) and Thornton et al. (2007) close to the mid-latitude tropopause under conditions with elevated water vapour and enhanced concentrations of condensation nuclei, such as sulphate particles. These observations were attributed to the occurrence of the heterogeneous reactions R1 ($ClONO_2$+HCl) and R2 ($ClONO_2 + H_2O$, Thornton et al., 2007; Keim et al., 1996). For the temperature and the water vapour range observed in the studies of Keim et al. (1996) (15 ppmv H_2O, ∼207 K) and Thornton et al. (2007) (15–22 ppmv H_2O, ∼213–215 K), a heterogeneous chlorine activation would not occur in the box-model simulation conducted here, not even in a sensitivity simulation assuming a high sulphate gas phase equivalent of 7.5 ppbv H_2SO_4 (not shown). At low temperatures ($\lesssim$196 K), heterogeneous chlorine activation may occur in the tropical stratosphere (Solomon et al., 2016; von Hobe et al., 2011). Von Hobe et al. (2011) observed enhanced ClO mixing ratios during aircraft campaigns over Australia (SCOUT-O_3, 2005) and Brazil (TROCCINOX, 2005) in combination with low temperatures and the occurrence of cirrus clouds. Analysing the balance between chlorine activation and deactivation von Hobe et al. (2011) showed an increase of the chlorine activation rate (R1) with a higher ClO, BrO and O_3 mixing ratio. Thus, once started, R1 accelerates due to higher ClO-mixing ratios subsequently yielding a fast conversion

of NO_x into HNO_3 (von Hobe et al., 2011), comparable to the NO_y repartitioning found in the present study. Von Hobe et al. (2011) found a threshold in ozone mixing ratio, which has to be exceeded for chlorine activation to occur. Hence, the water vapour threshold discussed here is expected to depend on the ozone mixing ratio, as well. Furthermore a potential occurrence of ice particles in the lowermost mid-latitude stratosphere (Spang et al., 2015) might affect the water vapour threshold due to a different heterogeneous reactivity on ice than on liquid particles.

An elevated sulphate content enhances the heterogeneous reaction rate caused by an increased liquid surface. Due to this relation, an impact of stratospheric albedo modification (by applying solar geoengineering) on the ozone loss process proposed by Anderson et al. (2012) is discussed (Dykema et al., 2014). Varying the sulphate content in this study showed that for temperatures and water vapour conditions of the case based on observations, a moderate enhancement of $3\times H_2SO_4$ is sufficient to yield ozone depletion. Considering the temperature and water vapour dependence of the chlorine activation line (Fig. 8, white line), a $10\times$ enhancement of stratospheric sulphate yields a shift of chlorine activation to slightly lower water vapour mixing ratios and higher temperatures. However, even for enhanced sulphate and a water vapour mixing ratio of 20 ppmv, the temperature has to fall below 205 K for chlorine activation (and hence ozone depletion) to occur at the assumed Cl_y and NO_y conditions of the standard case.

After the chlorine activation step, catalytic ozone loss cycles can occur: the ClO-Dimer cycle (**C1**), the ClO-BrO-cycle (**C2**) and cycles subsequent to R10 ($ClO + HO_2$, **C3**, **C5**–**C6**). Cycle **C3** is reported to have an impact on stratospheric ozone in mid-latitudes in previous studies (e.g. Johnson et al., 1995; Kovalenko et al., 2007; Ward and Rowley, 2016). Here, **C3** was found to be the dominate cycle based on R10 under standard conditions. Nevertheless, simulating the 0.5 Br_y and high Cl_y case has shown that the relevance of **C1** (ClO+ClO) and **C2** (ClO+BrO) depends on assumed initial values of Cl_y and Br_y. Anderson and Clapp (2018) discussed the occurrence of the ClO-Dimer cycle (**C1**) and the ClO-BrO-cycle (**C2**) dependent on water vapour, the Cl_y mixing ratio and temperature. They illustrate a significant increase in the rate of R4 (ClO+ClO) and R8 (ClO+BrO) if the combination of elevated water vapour and low temperatures is sufficient for chlorine activation to occur. If chlorine activation occurs in their model study, a higher Cl_y mixing ratio yields higher catalytic ozone loss rates (R4, R8). Their finding regarding the effect of temperature, water vapour and chlorine on the ozone loss process is consistent with the results found here. The occurrence of net chlorine activation is determined by temperature and water vapour mixing ratio, while the Cl_y mixing ratio controls how much ozone is destroyed.

A measure for the effect of temperature and water vapour on stratospheric chlorine activation and ozone chemistry is the temperature and water vapour dependent chlorine activation line (Fig. 8, white line). Anderson et al. (2012) estimates lower temperatures than 205 K as necessary for chlorine activation to occur at a water vapour mixing ratio of 20 ppmv and a climatological non enhanced sulphate content. In comparison, assuming standard conditions for Cl_y and NO_y but a constant temperature here, temperatures lower than 203 K are required for similar H_2O and sulphate concentrations. The standard trajectory was chosen here to hold for conditions most likely for chlorine activation based on SEAC^{4}RS measurements and at the temperature range of this trajectory, the measured water vapour mixing ratio (10.6 ppmv) is slightly lower than the water vapour threshold. Hence, for all SEAC^{4}RS and MACPEX trajectories calculated (not only the shown examples), no trajectory produced ozone loss. A further requirement for the occurrence of chlorine activation is the maintenance of the conditions,

which yield chlorine activation, during the entire time of chlorine activation. Assuming standard conditions and a water vapour mixing ratio of 20 ppmv, chlorine activation takes 5 hours, but for conditions of the water vapour threshold low temperatures and enhanced water vapour mixing ratios have to be maintained 24–36 hour for chlorine activation and thus an impact on stratospheric ozone chemistry to occur. For the occurrence of ozone depletion, temperatures have also to remain low and water vapour mixing ratios high after the chlorine activation step.

The maximum ozone depletion at standard conditions occurs here for a water vapour mixing ratio of 20 ppmv. Final ozone at 20 ppmv H_2O in the 7-day simulation is 11% lower than the final ozone reached under atmospheric background conditions of 5 ppmv H_2O. For the 19-day simulation at 20 ppmv H_2O, the final ozone is 22% reduced compared to the 19-day simulation at 5 ppmv H_2O. Anderson and Clapp (2018) calculated a similar ozone reduction of 17% in a 14-day simulation and the same potential temperature range of 380 K assuming 20 ppmv H_2O and similar Cl_y conditions as used here in the realistic case. In contrast assuming high Cl_y and NO_y of Anderson et al. (2012) in the case of high Cl_y would lead to an ozone loss of 85% (265 ppbv) during the 7-day simulation. This ozone loss would occur in the lower stratosphere. Borrmann et al. (1996, 1997) and Solomon et al. (1997) conducted a study about the impact of cirrus clouds on chlorine activation and ozone chemistry in the mid-latitudes lowermost stratosphere. They found a significant impact of heterogeneous processes occurring on cirrus clouds for ozone chemistry of the lowermost stratosphere but a minor effect for column ozone. Anderson and Clapp (2018) calculated a fractional loss in the total ozone column of 0.25% assuming a full Cl_y profile in the altitude range of 12–18 km with a constant water vapour mixing ratio of 20 ppmv and the mixing ratio of Cl_y similar to our standard case. However, the simulations assume a constant high water vapour mixing ratio and neglect mixing with the stratospheric background, which is characterized by much lower water vapour mixing ratios and subsequent dilution of convective uplifted air masses. Ozone loss would only occur in the specific volume of stratospheric air, that is directly affected by the convectively injected additional water. Hence, the ozone loss presented here corresponds to the maximal possible ozone loss for rather realistic convective overshooting conditions.

7 Conclusions

We investigated in detail the ozone loss mechanism at mid-latitudes in the lower stratosphere occurring under enhanced water vapour conditions and the sensitivity of this ozone loss mechanism on a variety of conditions. A CLaMS box-model study was conducted including a standard assumption and a variety of sensitivity cases regarding the chemical initialisation, temperatures and the duration of the simulated period. The assumed standard conditions (155.7 pptv Cl_y, 728.8 pptv NO_y, 197–203 K and an H_2SO_4 gas phase equivalent of 0.20 ppbv) were determined based on measurements in an H_2O environment showing strongly enhanced H_2O values compared to the stratospheric background during the SEAC^{4}RS aircraft campaign in Texas 2013.

The ozone loss mechanism consists of two phases: The first step is chlorine activation due to the heterogeneous reaction $ClONO_2 + HCl$ (R1), which yields both an increase of ClO_x and a decrease of NO_x. When chlorine is activated, enhanced ClO_x mixing ratios lead to catalytic ozone loss cycles in the second phase of the mechanism. Our findings show that besides

the ClO-Dimer-cycle (**C1**) and ClO-BrO-cycle (**C2**), three ozone loss cycles (**C3**, **C5**–**C6**) based on the reaction ClO+HO_2 (R10) have to be taken into account. The relevance of the cycles **C1**–**C3** and **C5**–**C6** for ozone loss depends on the water vapour, Cl_y and Br_y mixing ratios. Reduced NO_x mixing ratios yield a decreasing chemical net ozone formation in cycle **C4**. This reduced ozone formation at high water vapour mixing ratios is in the box-model simulation around 20% as high as the ozone destruction in catalytic ozone loss cycles. Furthermore a detailed analysis of chemical processes revealed the occurrence of pathways, which maintain high ClO_x and low NO_x mixing ratios after the chlorine activation step but do not reduce ozone, similar to HCl-null-cycles in the lower stratosphere (Müller et al., 2018) in Antarctic early spring.

Focussing on the dependence of chlorine activation on temperature and water vapour mixing ratio, we found that the temperature has to fall below 203 K for chlorine activation to occur at a water vapour mixing ratio of 20 ppmv and Cl_y and NO_y for our standard case. Testing the water vapour dependence of ozone loss along a realistic trajectory that experienced very low temperatures between 197 and 203 K, we observed a water vapour threshold of 11.0–11.6 ppmv H_2O, which has to be exceeded for ozone reduction to occur. For our assumed standard conditions, a maximum ozone loss of 9% (27 ppbv) was calculated for a water vapour mixing ratio of 20 ppmv. In contrast, a simulation assuming the observed conditions (10.6 ppmv H_2O) yielded ozone formation; but a tripling of background sulphate gas phase equivalent is sufficient for a slight ozone loss to occur under these unusually cold conditions for the chosen standard trajectory. Simulating a high Cl_y case assuming initial Cl_y and NO_y based on the study of Anderson et al. (2012) results in both a lower water vapour threshold of 7–8 ppmv and a larger ozone depletion of 85% (265 ppbv) at high water vapour mixing ratios. The model runs described here assume an air parcel moving along the trajectory and does not mix with neighbouring air masses. In the case of water, this would likely reduce the concentration. Because that mixing was neglected, the runs discussed here are likely and extreme case, and the ozone loss modelled provides an upper bound to the process described.

Considering the duration for which low temperatures and high water vapour mixing ratios have to be maintained to activate chlorine and deplete stratospheric ozone, a chlorine activation time of 24 to 36 hours when the water vapour abundance is near the threshold and of 5 h at 20 ppmv H_2O was calculated. The water vapour threshold shifts strongly with changing temperature and sulphate content as well as with Cl_y, NO_y and Br_y mixing ratios. The dependence of the water vapour threshold is explained here by focussing on the water dependence of the heterogeneous reactivity (R1) and the balance between heterogeneous chlorine activation (R1, $ClONO_2 + HCl$) and gas phase chlorine deactivation (R24, $Cl + CH_4$).

The ozone loss mechanism was investigated here by conducting box-model simulations along a trajectory, which was calculated based on measurements of elevated water vapour. Sensitivity and case studies, which cover a range of uncertainties, illustrate the impact of the Cl_y, NO_y, Br_y and H_2O mixing ratio, the temperature, the sulphate gas equivalent and the duration of the simulated period on the ozone loss process. While the water vapour threshold which has to be exceeded for chlorine activation to occur is mainly determined by the temperature, water vapour mixing ratio and sulphate content, the intensity of ozone loss depends on Cl_y, NO_y, Br_y and the duration of the time period, for which a chlorine activation can be maintained. Our comprehensive sensitivity studies are a basis to assess the impact of enhanced water vapour mixing ratios in the lower mid-latitude stratosphere on ozone under sulphate geoengineering conditions and in a changing climate. However, we did not

Atmos. Chem. Phys. Discuss., https://doi.org/10.5194/acp-2018-1193
Manuscript under review for journal Atmos. Chem. Phys.
Discussion started: 12 December 2018

simulate ozone depletion for the observed conditions. Further global modelling studies are needed to establish whether the mechanism analysed here is of concern for the future.

Code and data availability. The complete SEAC^{4}RS data ar availiable at https://www-air.larc.nasa.gov/cgi-bin/ArcView/seac4rs. The CLaMS box model calculations can be requested from Sabine Robrecht (sa.robrecht@fz-juelich.de).

Appendix A: Tracer-Tracer Correlations

The mixing ratios of Cl_y and NO_y were initialized based on stratospheric tracer-tracer correlations from Grooß et al. (2014). Cl_y and NO_y were initialized based on a CH_4 measurement during the SEAC^{4}RS aircraft campaign. Initial Cl_y was calculated using the tracer-tracer correlation (Grooß et al., 2014)

$$[Cl_y] = 2.510 + 3.517 \cdot [CH_4] - 3.741 \cdot [CH_4]^2 + 0.4841 \cdot [CH_4]^3 + 0.03042 \cdot [CH_4]^4. \quad \text{(A1)}$$

The volume mixing ratio of Cl_y ($[Cl_y]$) is here in ppt and the mixing ratio of methane ($[CH_4]$) in ppm.
To determine NO_y based on the CH_4 measurement, first N2O was calculated through

$$[N_2O] = -124.9 + 311.9 \cdot [CH_4] - 158.1 \cdot [CH_4]^2 + 146.6 \cdot [CH_4]^3 - 43.92 \cdot [CH_4]^4 \quad \text{(A2)}$$

assuming $[N_2O]$ in ppbv and $[CH_4]$ in ppmv (Grooß et al., 2002). Subsequently NO_y (in ppt) was calculated in a correlation with N_2O.

$$[NO_y] = 11.57 + 0.1235 \cdot [N_2O] - 1.013 \cdot 10^{-3} \cdot [N_2O]^2 + 1.984 \cdot 10^{-6} \cdot [N_2O]^3 - 1.119 \cdot 10^{-9} \cdot [N_2O]^4 \quad \text{(A3)}$$

In the MACPEX case NO_y and Cl_y were initialized based on N_2O measurements. NO_y was calculated using correlation A3. Cl_y was calculated using A1. Therefore first CH_4 (im ppmv) had to be calculated based on a correlation with N_2O (in ppbv) (Grooß et al., 2014).

$$[CH_4] = 0.1917 + 0.01333 \cdot [N_2O] - 8.239 \cdot 10^{-5} \cdot [N_2O]^2 + 2.840 \cdot 10^{-7} \cdot [N_2O]^3 - 3.376 \cdot 10^{-10} \cdot [N_2O]^4 \quad \text{(A4)}$$

Competing interests. The authors declare that they have no conflict of interest.

Acknowledgements. Our activities were funded by the German Science Foundation (Deutsche Forschungsgemeinschaft, DFG) under the DFG project CE-O_3 in the context of the Priority Program Climate Engineering: Risks, Challenges, Opportunities? (SPP 1689; VO 1276/4-1). We thank the European Centre for Medium-Range Weather Forecasts (ECMWF) for providing ERA-Interim data. We thank the group of Steven Wofsy (Havard University, Department Earth and Planetary Science, Cambridge, MA USA) and Jessica Smith for providing their data measured during the SEAC^{4}RS aircraft campaign.

References

Anderson, J. G. and Clapp, C. E.: Coupling free radical catalysis, climate change, and human health, Phys. Chem. Chem. Phys., 20, 10 569–10 587, https://doi.org/10.1039/C7CP08331A, 2018.

Anderson, J. G., Wilmouth, D. M., Smith, J. B., and Sayres, D. S.: UV Dosage Levels in Summer: Increased Risk of Ozone Loss from Convectively Injected Water Vapor, Science, 337, 835–839, https://doi.org/10.1126/science.1222978, 2012.

Anderson, J. G., Weisenstein, D. K., Bowman, K. P., Homeyer, C. R., Smith, J. B., Wilmouth, D. M., Sayres, D. S., Klobas, J. E., Leroy, S. S., Dykema, J. A., and Wofsy, S. C.: Stratospheric ozone over the United States in summer linked to observations of convection and temperature via chlorine and bromine catalysis, Proc. Natl. Acad. Sci., 114, E4905–E4913, https://doi.org/10.1073/pnas.1619318114, 2017.

Becker, G., Grooß, J.-U., McKenna, D. S., and Müller, R.: Stratospheric photolysis frequencies: Impact of an improved numerical solution of the radiative transfer equation, J. Atmos. Chem., 37, 217–229, https://doi.org/10.1023/A:1006468926530, 2000.

Berthet, G., Jégou, F., Catoire, V., Krysztofiak, G., Renard, J.-B., Bourassa, A. E., Degenstein, D. A., Brogniez, C., Dorf, M., Kreycy, S., Pfeilsticker, K., Werner, B., Lefèvre, F., Roberts, T. J., Lurton, T., Vignelles, D., Begue, N., Bourgeois, Q., Daugeron, D., Cartiert, M., Robert, C., Gaubicher, B., and Guimbaud, C.: Impact of a moderate volcanic eruption on chemistry in the lower stratosphere: balloon-borne observations and model calculations, Atmos. Chem. Phys., 17, 2229–2253, https://doi.org/10.5194/acp-17-2229-2017, 2017.

Borrmann, S., Solomon, S., Dye, J. E., and Luo, B.: The potential of cirrus clouds for heterogeneous chlorine activation, Geophys. Res. Lett., 23, 2133–2136, https://doi.org/10.1029/96GL01957, 1996.

Borrmann, S., Solomon, S., Avallone, L., Toohey, D., and Baumgardner, D.: On the occurrence of ClO in cirrus clouds and volcanic aerosol in the tropopause region, Geophys. Res. Lett., 24, 2011–2014, https://doi.org/10.1029/97GL02053, 1997.

Brewer, A. W.: Evidence for a world circulation provided by the measurements of helium and water vapour distribution in the stratosphere, Q. J. R. Meteorol. Soc., 75, 351–363, https://doi.org/10.1002/qj.49707532603, 1949.

Brown, P. N., Byrne, G. D., and Hindmarsh, A. C.: VODE: A variable coefficient ODE solver, SIAM J. Sci. Stat. Comput., 10, 1038–1051, https://doi.org/https://doi.org/10.1137/0910062, 1989.

Crutzen, P. J., Müller, R., Brühl, C., and Peter, T.: On the potential importance of the gas phase reaction $CH_3O_2 + ClO \rightarrow ClOO + CH_3O$ and the heterogeneous reaction $HOCl + HCl \rightarrow H_2O + Cl_2$ in "ozone hole" chemistry, Geophys. Res. Lett., 19, 1113–1116, https://doi.org/10.1029/92GL01172, 1992.

Daniel, J. S., Solomon, S., Portmann, R. W., and Garcia, R. R.: Stratospheric ozone destruction: The importance of bromine relative to chlorine, J. Geophys. Res., 104, 23 871–23 880, https://doi.org/10.1029/1999JD900381, 1999.

Dee, D. P., Uppala, S. M., Simmons, A. J., Berrisford, P., Poli, P., Kobayashi, S., Andrae, U., Balmaseda, M. A., Balsamo, G., Bauer, P., Bechtold, P., Beljaars, A. C. M., van de Berg, L., Bidlot, J., Bormann, N., Delsol, C., Dragani, R., Fuentes, M., Geer, A. J., Haimberger, L., Healy, S. B., Hersbach, H., Hólm, E. V., Isaksen, L., Kållberg, P., Köhler, M., Matricardi, M., McNally, A. P., Monge-Sanz, B. M., Morcrette, J.-J., Park, B.-K., Peubey, C., de Rosnay, P., Tavolato, C., Thépaut, J.-N., and Vitart, F.: The ERA-Interim reanalysis: configuration and performance of the data assimilation system, Q. J. R. Meteorol. Soc., 137, 553–597, https://doi.org/10.1002/qj.828, 2011.

Drdla, K. and Müller, R.: Temperature thresholds for chlorine activation and ozone loss in the polar stratosphere, Ann. Geophys., 30, 1055–1073, https://doi.org/10.5194/angeo-30-1055-2012, 2012.

Dykema, J. A., Keith, D. W., Anderson, J. G., and Weisenstein, D.: Stratospheric controlled pertubation experiment: a small-scale experiment to improve understanding of the risks of solar geoengineering, Phil. Trans. R. Soc. A, 372, 1–22, https://doi.org/10.1098/rsta.2014.0059, 2014.

Gao, R. S., Ballard, J., Watts, L. A., Thornberry, T. D., Ciciora, S. J., McLaughlin, R. J., and Fahey, D. W.: A compact, fast UV photometer for measurement of ozone from research aircraft, Atmos. Meas. Tech., 5, 2201–2210, https://doi.org/10.5194/amt-5-2201-2012, 2012.

GHG Bulletin, ed.: WMO Greenhouse Gas Bulletin, GHG Bulletin No.10, WMO, http://www.wmo.int/pages/prog/arep/gaw/ghg/GHGbulletin.html, 2014.

Grenfell, J. L., Lehmann, R., Mieth, P., Langematz, U., and Steil, B.: Chemical reaction pathways affecting stratospheric and mesospheric ozone, J. Geophys. Res. A, 111, https://doi.org/10.1029/2004JD005713, 2006.

Grooß, J.-U., Günther, G., Konopka, P., Müller, R., McKenna, D. S., Stroh, F., Vogel, B., Engel, A., Müller, M., Hoppel, K., Bevilacqua, R., Richard, E., Webster, C. R., Elkins, J. W., Hurst, D. F., Romashkin, P. A., and Baumgardner, D. G.: Simulation of ozone depletion in spring 2000 with the Chemical Lagrangian Model of the Stratosphere (CLaMS), J. Geophys. Res., 107, 8295, https://doi.org/10.1029/2001JD000456, 2002.

Grooß, J.-U., Brautzsch, K., Pommrich, R., Solomon, S., and Müller, R.: Stratospheric ozone chemistry in the Antarctic: What controls the lowest values that can be reached and their recovery?, Atmos. Chem. Phys., 11, 12 217–12 226, https://doi.org/10.5194/acp-11-12217-2011, 2011.

Grooß, J.-U., Engel, I., Borrmann, S., Frey, W., Günther, G., Hoyle, C. R., Kivi, R., Luo, B. P., Molleker, S., Peter, T., Pitts, M. C., Schlager, H., Stiller, G., Vömel, H., Walker, K. A., and Müller, R.: Nitric acid trihydrate nucleation and denitrification in the Arctic stratosphere, Atmos. Chem. Phys., 14, 1055–1073, https://doi.org/10.5194/acp-14-1055-2014, 2014.

Haagen-Smit, A. H.: Chemistry and physiology of the Los Angeles photochemical smog, Ind. Eng. Chem., 44, 1342–1346, https://doi.org/10.1021/ie50510a045, 1952.

Hanisco, T. F., Moyer, E. J., Weinstock, E. M., Clair, J. M. S., Sayres, D. S., Smith, J. B., Lockwood, R., Anderson, J. G., Dessler, A. E., Keutsch, F. N., Spackman, J. R., Read, W. G., and Bui, T. P.: Observations of deep convective influence on stratospheric water vapor and its isotopic composition, Geophys. Res. Lett., 34, L04814, https://doi.org/10.1029/2006GL027899, 2007.

Herman, R. L., Ray, E. A., Rosenlof, K. H., Bedka, K. M., Schwartz, M. J., Read, W. G., Troy, R. F., Chin, K., Christensen, L. E., Fu, D., Stachnik, R. A., Bui, T. P., and Dean-Day, J. M.: Enhanced stratospheric water vapor over the summertime continental United States and the role of overshooting convection, Atmos. Chem. Phys., 17, 6113, https://doi.org/10.5194/acp-17-6113-2017, 2017.

Homeyer, C. R., Pan, L. L., Dorsi, S. W., Avallone, L. M., Weinheimer, A. J., O'Brien, A. S., DiGangi, J. P., Zondlo, M. A., Ryerson, T. B., Diskin, G. S., and Campos, T. L.: Convective transport of water vapor into the lower stratosphere observed during double-tropopause events, J. Geophys. Res., 119, 10 941–10 958, https://doi.org/10.1002/2014JD021485, 2014.

Johnson, D. G., Traub, W. A., Chance, K. V., Jucks, K. W., and Stachnik, R. A.: Estimating the abundance of ClO from simultaneous remote sensing measurements of HO2, OH, and HOCl, Geophys. Res. Lett., 22, 1869–1871, https://doi.org/10.1029/95GL01249, 1995.

Keim, E. R., Fahey, D. W., Negro, L. A. D., Woodbridge, E. L., Gao, R., Wennberg, P. O., Cohen, R. C., Stimpfle, R. M., Kelly, K. K., Hintsa, E. J., Wilson, J. C., Jonsson, H. H., Dye, J. E., Baumgardner, D. G., Kawa, S. R., Salawitch, R. J., Proffitt, M. H., Loewenstein, M., Podolske, J. R., and Chan, K. R.: Observations of large reductions in the NO/NO_y ratio near the mid-latitude tropopause and the role of heterogeneous chemistry, Geophys. Res. Lett., 23, 3223–3226, https://doi.org/10.1029/96GL02593, 1996.

Klooster, S. L. V. and Roebber, P. J.: Surface-Based Convective Potential in the Contiguous United States in a Business-as-Usual Future Climate, J. Climate, 22, 3317–3330, https://doi.org/10.1175/2009JCLI2697.1, 2009.

Koenig, T. K., Volkamer, R., Baidar, S., Dix, B., Wang, S., Anderson, D. C., Salawitch, R. J., Wales, P. A., Cuevas, C. A., Fernandez, R. P., Saiz-Lopez, A., Evans, M. J., Sherwen, T., Jacob, D. J., Schmidt, J., Kinnison, D., Lamarque, J.-F., Apel, E. C., Bresch, J. C., Campos, T., Flocke, F. M., Hall, S. R., Honomichl, S. B., Hornbrook, R., Jensen, J. B., Lueb, R., Montzka, D. D., Pan, L. L., Reeves, J. M., Schauffler, S. M., Ullmann, K., Weinheimer, A. J., Atlas, E. L., Donets, V., Navarro, M. A., Riemer, D., Blake, N. J., Chen, D., Huey, L. G., Tanner, D. J., Hanisco, T. F., and Wolfe, G. M.: BrO and inferred Br_y profiles over the western Pacific: relevance of inorganic bromine sources and a Br_y minimum in the aged tropical tropopause layer, Atmos. Chem. Phys., 17, 15 245–15 270, https://doi.org/10.5194/acp-17-15245-2017, 2017.

Konopka, P., Ploeger, F., Tao, M., Birner, T., and Riese, M.: Hemispheric asymmetries and seasonality of mean age of air in the lower stratosphere: Deep versus shallow branch of the Brewer-Dobson circulation, J. Geophys. Res., 120, 2053–2066, https://doi.org/10.1002/2014JD022429, 2015.

Kovalenko, L. J., Jucks, K. W., Salawitch, R. J., Toon, G. C., Blavier, J.-F., Johnson, D. G., Kleinböhl, A., Livesey, N. J., Margitan, J. J., Pickett, H. M., Santee, M. L., Sen, B., Stachnik, R. A., and Waters, J. W.: Observed and modeled HOCl profiles in the midlatitude stratosphere: Implication for ozone loss, Geophys. Res. Lett., 34, https://doi.org/10.1029/2007GL031100, 2007.

LeTexier, H., Solomon, S., and Garcia, R. R.: The role of molecular hydrogen and methane oxidation in the water vapour budget of the stratosphere, Q. J. R. Meteorol. Soc., 114, 281 – 295, https://doi.org/https://doi.org/10.1002/qj.49711448002, 1988.

McElroy, M. B., Salawitch, R. J., Wofsy, S. C., and Logan, J. A.: Reductions of Antarctic Ozone due to Synergistic Interactions of Chlorine and Bromine, Nature, 321, 759–762, https://doi.org/10.1038/321759a0, 1986.

McKenna, D. S., Grooß, J.-U., Günther, G., Konopka, P., Müller, R., Carver, G., and Sasano, Y.: A new Chemical Lagrangian Model of the Stratosphere (CLaMS): 2. Formulation of chemistry scheme and initialization, J. Geophys. Res., 107, 4256, https://doi.org/10.1029/2000JD000113, 2002a.

McKenna, D. S., Konopka, P., Grooß, J.-U., Günther, G., Müller, R., Spang, R., Offermann, D., and Orsolini, Y.: A new Chemical Lagrangian Model of the Stratosphere (CLaMS): 1. Formulation of advection and mixing, J. Geophys. Res., 107, 4309, https://doi.org/10.1029/2000JD000114, 2002b.

Meyer, J., Rolf, C., Schiller, C., Rohs, S., Spelten, N., Afchine, A., Zöger, M., Sitnikov, N., Thornberry, T. D., Rollins, A. W., Bozóki, Z., Tátrai, D., Ebert, V., Kühnreich, B., Mackrodt, P., Möhler, O., Saathoff, H., Rosenlof, K. H., and Krämer, M.: Two decades of water vapor measurements with the FISH fluorescence hygrometer: a review, Atmos. Chem. Phys., 15, 8521–8538, https://doi.org/10.5194/acp-15-8521-2015, 2015.

Molina, L. T. and Molina, M. J.: Production of Cl_2O_2 from the self-reaction of the ClO radical, J. Phys. Chem., 91, 433–436, https://doi.org/10.1021/j100286a035, 1987.

Molina, M. J., Tso, T.-L., Molina, L. T., and Wang, F. C.-Y.: Antarctic Stratospheric Chemistry of Chlorine Nitrate, Hydrogen Chloride, and Ice: Release of Active Chlorine, Science, 238, 1253–1257, https://doi.org/10.1126/science.238.4831.1253, 1987.

Müller, R., Grooß, J.-U., Zafar, A., Robrecht, S., and Lehmann, R.: The maintenance of elevated active chlorine levels in the Antarctic lower stratosphere through HCl null cycles, Atmos. Chem. Phys., 18, 2985–2997, https://doi.org/10.5194/acp-18-2985-2018, 2018.

Navarro, M. A., Saiz-Lopez, A., Cuevas, C. A., Fernandez, R. P., Atlas, E., Rodriguez-Lloveras, X., Kinnison, D., Lamarque, J.-F., Tilmes, S., Thornberry, T., Rollins, A., Elkins, J. W., Hintsa, E. J., and Moore, F. L.: Modeling the inorganic bromine partitioning in the tropical tropopause layer over the eastern and western Pacific Ocean, Atmos. Chem. Phys., 17, 9917–9930, https://doi.org/10.5194/acp-17-9917-2017, 2017.

Pitari, G., Visioni, D., Mancini, E., Cionni, I., Di Genova, G., and Gandolfi, I.: Sulfate aerosols from non-explosive volcanoes: chemical-radiative effects in the troposphere and lower stratosphere, Atmosphere, 7, 85, https://doi.org/10.3390/atmos7070085, 2016.

Ploeger, F., Konopka, P., Günther, G., Grooß, J.-U., and Müller, R.: Impact of the vertical velocity scheme on modeling transport across the tropical tropopause layer, J. Geophys. Res., 115, D03301, https://doi.org/10.1029/2009JD012023, 2010.

Poshyvailo, L., Müller, R., Konopka, P., Günther, G., Riese, M., Podglajen, A., and Ploeger, F.: Sensitivities of modelled water vapour in the lower stratosphere: temperature uncertainty, effects of horizontal transport and small-scale mixing, Atmos. Chem. Phys., 18, 8505–8527, https://doi.org/10.5194/acp-18-8505-2018, 2018.

Prather, M. J.: More rapid ozone depletion through the reaction of HOCl with HCl on polar stratospheric clouds, Nature, 355, 534–537, https://doi.org/10.1038/355534a0, 1992.

Randel, W. J., Wu, F., Oltmans, S. J., Rosenlof, K. H., and Nodoluha, G. E.: Interannual Changes of Stratospheric Water Vapor and Correlations with Tropical Tropopause Temperatures, J. Atmos. Sci., 61, 2133–2148, https://doi.org/10.1175/1520-0469(2004)061<2133:ICOSWV>2.0.CO;2, 2004.

Ravishankara, A. R.: Water Vapor in the Lower Stratosphere, Science, 337, 809–810, https://doi.org/10.1126/science.1227004, 2012.

Rohs, S., Schiller, C., Riese, M., Engel, A., Schmidt, U., Wetter, T., Levin, I., Nakazawa, T., and Aoki, S.: Long-term changes of methane and hydrogen in the stratosphere in the period 1978 – 2003 and their impact on the abundance of stratospheric water vapor, J. Geophys. Res., 111, D14315, https://doi.org/10.1029/2005JD006877, 2006.

Rollins, A. W., Thornberry, T. D., Gao, R. S., Smith, J. B., Sayres, D. S., Sargent, M. R., Schiller, C., Krämer, M., Spelten, N., Hurst, D. F., Jordan, A. F., Hall, E. G., Vomel, H., Diskin, G. S., Podolske, J. R., Christensen, L. E., Rosenlof, K. H., and Fahey, D. W.: Evaluation of UT/LS hygrometer accuracy by intercomparison during the NASA MACPEX mission, J. Geophys. Res. A, 119, 1915–1935, https://doi.org/10.1002/2013JD020817, 2014.

Sander, S. P., Friedl, R. R., Barker, J. R., Golden, D. M., Kurylo, M. J., Wine, P. H., Abbatt, J. P. D., Burkholder, J. B., Kolb, C. E., Moortgat, G. K., Huie, R. E., and Orkin, V. L.: Chemical kinetics and photochemical data for use in atmospheric studies, JPL Publication 10-6, 2011.

Schiller, C., Grooß, J.-U., Konopka, P., Plöger, F., Silva dos Santos, F. H., and Spelten, N.: Hydration and dehydration at the tropical tropopause, Atmos. Chem. Phys., 9, 9647–9660, https://doi.org/10.5194/acp-9-9647-2009, 2009.

Schwartz, M. J., Read, W. G., Santee, M. L., Livesesy, N. J., Froidevaux, L., Lamert, A., and Manney, G. L.: Convectively injected water vapor in the North American summer lowermost stratosphere, Geophys. Res. Lett., 40, 2316–2321, https://doi.org/10.1002/grl.50421, 2013.

Shi, Q., Jayne, J. T., Kolb, C. E., Worsnop, D. R., and Davidovits, P.: Kinetic model for reaction of $ClONO_2$ with H_2O and HCl and HOCl with HCl in sulfuric acid solutions, J. Geophys. Res., 106, 24 259–24 274, https://doi.org/10.1029/2000JD000181, 2001.

Smith, J. B., Wilmouth, D. M., Bedka, K. M., Bowman, K. P., Homeyer, C. R., Dykema, J. A., Sargent, M. R., Clapp, C. E., Leroy, S. S., Sayres, D. S., Dean-Day, J. M., Bui, T. P., and Anderson, J. G.: A case study of convectively sourced water vapor observed in the overworld stratosphere over the United States, J. Geophys. Res., 122, 9529–9554, https://doi.org/10.1002/2017JD026831, 2017.

Solomon, S.: Stratospheric ozone depletion: A review of concepts and history, Rev. Geophys., 37, 275–316, https://doi.org/10.1029/1999RG900008, 1999.

Solomon, S., Garcia, R. R., Rowland, F. S., and Wuebbles, D. J.: On the depletion of Antarctic ozone, Nature, 321, 755–758, https://doi.org/10.1038/321755a0, 1986.

Solomon, S., Borrmann, S., Garcia, R. R., Portmann, R., Thomason, L., Poole, L. R., Winker, D., and McCormick, M. P.: Heterogeneous chlorine chemistry in the tropopause region, J. Geophys. Res., 102, 21 411–21 429, 1997.

Solomon, S., Kinnison, D., Garcia, R. R., Bandoro, J., Mills, M., Wilka, C., Neely III, R. R., Schmidt, A., Barnes, J. E., Vernier, J.-P., and Hoepfner, M.: Monsoon circulations and tropical heterogeneous chlorine chemistry, Geophys. Res. Lett., 43, https://doi.org/10.1002/2016GL071778, 2016.

Spang, R., Günther, G., Riese, M., Hoffmann, L., Müller, R., and Griessbach, S.: Satellite observations of cirrus clouds in the Northern Hemisphere lowermost stratosphere, Atmos. Chem. Phys., 15, 927–950, https://doi.org/10.5194/acp-15-927-2015, 2015.

Spang, R., Hoffmann, L., Müller, R., Grooß, J.-U., Tritscher, I., Höpfner, M., Pitts, M., Orr, A., and Riese, M.: A climatology of polar stratospheric cloud composition between 2002 and 2012 based on MIPAS/Envisat observations, Atmos. Chem. Phys., 18, 5089–5113, https://doi.org/10.5194/acp-18-5089-2018, 2018.

Thomason, L. W. and Peter, T., eds.: SPARC Assessment of Stratospheric Aerosol Properties, SPARC Report No. 4, WCRP-124, WMO/TD-No.1295, http://www.atmosp.physics.utoronto.ca/SPARC/index.html, 2006.

Thomason, L. W., Poole, L. R., and Deshler, T.: A global climatoloy of stratospheric aerosol surface area density deduced from Stratospheric Aerosol and Gas Experiment II measurements: 1984-1994, J. Geophys. Res., 102, 8967–8976, https://doi.org/10.1029/96JD02962, 1997.

Thornton, B. F., Toohey, D. W., Tuck, A. F., Elkins, J. W., Kelly, K. K., Hovde, S. J., Richard, E. C., Rosenlof, K. H., Thompson, T. L., Mahoney, M. J., and Wilson, J. C.: Chlorine activation near the midlatitude tropopause, J. Geophys. Res., 112, D18 306, https://doi.org/10.1029/2006JD007640, 2007.

Toon, O. B., Maring, H., Dibb, J., Ferrare, R., Jacob, D. J., Jensen, E. J., Luo, Z. J., Mace, G. G., Pan, L. L., Pfister, L., Rosenlof, K. H., Redemann, J., Reid, J. S., Singh, H. B., Thompson, A. M., Yokelson, R., Minnis, P., Chen, G., Jucks, K. W., and Pszenny, A.: Planning, implementation, and scientific goals of the Studies of Emissions and Atmospheric Composition, Clouds and Climate Coupling by Regional Surveys (SEAC4RS) field mission, J. Geophys. Res. A, 121, 4967–5009, https://doi.org/10.1002/2015JD024297, 2016.

Trapp, R. J., Diffenbaugh, N. S., and Gluhovsky, A.: Transient response of severe thunderstorm forcing to elevated greenhouse gas concentrations, Geophys. Res. Lett., 36, https://doi.org/10.1029/2008GL036203, 2009.

Vogel, B., Feck, T., and Grooß, J.-U.: Impact of stratospheric water vapor enhancements caused by CH_4 and H_2 increase on polar ozone loss, J. Geophys. Res., 116, D05301, https://doi.org/10.1029/2010JD014234, 2011.

Vogel, B., Günther, G., Müller, R., Grooß, J.-U., and Riese, M.: Impact of different Asian source regions on the composition of the Asian monsoon anticyclone and of the extratropical lowermost stratosphere, Atmos. Chem. Phys., 15, 13 699–13 716, https://doi.org/10.5194/acp-15-13699-2015, 2015.

Vogel, B., Günther, G., Müller, R., Grooß, J.-U., Afchine, A., Bozem, H., Hoor, P., Krämer, M., Müller, S., Riese, M., Rolf, C., Spelten, N., Stiller, G. P., Ungermann, J., and Zahn, A.: Long-range transport pathways of tropospheric source gases originating in Asia into the northern lower stratosphere during the Asian monsoon season 2012, Atmos. Chem. Phys., 16, 15 301–15 325, https://doi.org/10.5194/acp-16-15301-2016, 2016.

von Hobe, M., Grooß, J.-U., Günther, G., Konopka, P., Gensch, I., Krämer, M., Spelten, N., Afchine, A., Schiller, C., Ulanovsky, A., Sitnikov, N., Shur, G., Yushkov, V., Ravegnani, F., Cairo, F., Roiger, A., Voigt, C., Schlager, H., Weigel, R., Frey, W., Borrmann, S., Müller, R., and Stroh, F.: Evidence for heterogeneous chlorine activation in the tropical UTLS, Atmos. Chem. Phys., 11, 241–256, https://doi.org/10.5194/acp-11-241-2011, 2011.

Wales, P. A., Salawitch, R. J., Nicely, J. M., Anderson, D. C., Canty, T. P., Baidar, S., Dix, B., Koenig, T. K., Volkamer, R., Chen, D., Huey, L. G., Tanner, D. J., Cuevas, C. A., Fernandez, R. P., Kinnison, D. E., Lamarque, J.-F., Saiz-Lopez, A., Atlas, E. L., Hall, S. R., Navarro, M. A., Pan, L. L., Schauffler, S. M., Stell, M., Tilmes, S., Ullmann, K., Weinheimer, A. J., Akiyoshi, H., Chipperfield, M. P., Deushi, M., Dhomse, S. S., Feng, W., Graf, P., Hossaini, R., Jöckel, P., Mancini, E., Michou, M., Morgenstern, O., Oman, L. D., Pitari, G., Plummer,

D. A., Revell, L. E., Rozanov, E., Saint-Martin, D., Schofield, R., Stenke, A., Stone, K. A., Visioni, D., Yamashita, Y., and Zeng, G.: Stratospheric Injection of Brominated Very Short-Lived Substances: Aircraft Observations in the Western Pacific and Representation in Global Models, J. Geophys. Res. A, 123, 5690–5719, https://doi.org/10.1029/2017JD027978, 2018.

Ward, M. K. M. and Rowley, D. M.: Kinetics of the ClO + CH_3O_2 reaction over the temperature range T=250–298 K, Phys. Chem. Chem. Phys., 18, 13 646–13 656, https://doi.org/10.1039/c6cp00724d, 2016.

Webster, C. R., May, R. D., Trimble, C. A., Chave, R. G., and Kendall, J.: Aircraft laser infrared absorption spectrometer (ALIAS) for in situ atmospheric measurements of HCl, N_2O, CH_4, NO_2, and HNO_3, Appl. Opt., 33, 454–472, https://doi.org/10.1364/AO.33.000454, 1994.

Weinstock, E. M., Smith, J. B., Sayres, D. S., Pittman, J. V., Spackman, J. R., Hintsa, E. J., Hanisco, T. F., Moyer, E. J., St Clair, J. M., Sargent, M. R., and Anderson, J. G.: Validation of the Harvard Lyman-α in situ water vapor instrument: Implications for the mechanisms that control stratospheric water vapor, J. Geophys. Res. A, 114, https://doi.org/10.1029/2009JD012427, 2009.

Werner, B., Stutz, J., Spolaor, M., Scalone, L., Raecke, R., Festa, J., Colosimo, S. F., Cheung, R., Tsai, C., Hossaini, R., Chipperfield, M. P., Taverna, G. S., Feng, W., Elkins, J. W., Fahey, D. W., Gao, R.-S., Hintsa, E. J., D., T. T., Lee Moore, F., Navarro, M. A., Atlas, E., Daube, B. C., Pittman, J., Wofsy, S., and Pfeilsticker, K.: Probing the subtropical lowermost stratosphere and the tropical upper troposphere and tropopause layer for inorganic bromine, Atmos. Chem. Phys., 17, 1161–1186, https://doi.org/10.5194/acp-17-1161-2017, 2017.

WMO: Scientific assessment of ozone depletion: 2014, Global Ozone Research and Monitoring Project–Report No. 55, Geneva, Switzerland, 2014.

Zafar, A. M., Müller, R., Grooss, J.-U., Robrecht, S., Vogel, B., and Lehmann, R.: The relevance of reactions of the methyl peroxy radical (CH3O2) and methylhypochlorite (CH3OCl) for Antarctic chlorine activation and ozone loss, Tellus B, 70, 1507 391, https://doi.org/10.1080/16000889.2018.1507391, 2018.